Charles University in Prague

Faculty of Science

Ph.D. study program: Inorganic Chemistry
Field of study: Inorganic Chemistry

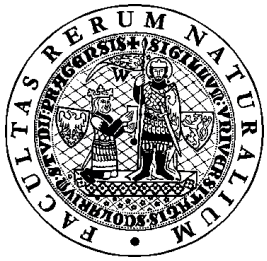

Mgr. Bohuslav Drahoš

Potenciální kontrastní látky pro MRI založené na komplexech manganu(II)

Potential contrast agents for MRI based on manganese(II) complexes

Ph.D. Thesis

Supervisors: Prof. RNDr. Ivan Lukeš, CSc.
Dr. Eva Jakab Tóth

Prague 2011

ÉCOLE DOCTORALE SCIENCES ET TECHNOLOGIES

Centre de Biophysique Moléculaire, CNRS, Orléans /

Departement of Inorganic Chemistry, Charles University in Prague

THÈSE EN COTUTELLE INTERNATIONALE présentée par :

Bohuslav DRAHOŠ

soutenue le : **23 septembre 2011**

pour obtenir le grade de :
Docteur de l'université d'Orléans et de l l'université d'Charles à Prague

Discipline : Chimie Inorganique

Potential contrast agents for MRI based on manganese(II) complexes

THÈSE dirigée par :

Mme. Eva JAKAB TÓTH	Dr., CBM, CNRS, Orléans
M. Ivan LUKEŠ	Prof. RNDr., CSc., Université de Charles a Prague

RAPPORTEURS :

M. Imre TÓTH	Prof., Université de Debrecen
M. Carlos F.G.C. GERALDES	Prof., Université de Coimbra

JURY:

M. Ivan NĚMEC	Doc. RNDr., PhD., Université de Charles a Prague, président du jury
M. Ivan LUKEŠ	Prof. RNDr., CSc., Université de Charles a Prague, directeur thèse
Mme. Eva JAKAB TÓTH	Dr., CBM, CNRS, Orléans, directrice thèse
M. Stéphane PETOUD	Prof., Université de Orléans
M. Carlos F.G.C. GERALDES	Prof., Université de Coimbra, rapporteur
M. Imre TÓTH	Prof., Université de Debrecen, rapporteur

Declaration:

I declare that this Thesis is my original work except as cited in the references. The Thesis has not been submitted, or is being currently submitted, for any other academic degree.

In Prague, 10.06.2011

Bohuslav Drahoš

Signature:

Table of Contents

Abstract

The thesis is focused on the synthesis and characterization of novel Mn^{2+} complexes as alternative to Gd^{3+} chelates which are wide-spread contrast agents in Magnetic Resonance Imaging (MRI). In the perspective to find suitable chelators of Mn^{2+}, three groups of pentadentate ligands with different size of macrocylic cavity, different donor atoms and number of pendant arms containing various functional groups have been investigated. Coordination numbers of 6 or 7 were found in the crystal structure of the Mn^{2+} complexes enabling binding of one or two water molecules in the first coordination sphere. The direct water coordination causes a decrease in the complex stability and thus, the thermodynamic stability of investigated chelates is lower than that of polyaminocarboxylate complexes and their dissociation is very fast in comparison to [Mn(nota)] and $[Mn(dota)]^{2-}$. The studied Mn^{2+} complexes do not undergo oxidation in air except for complexes with 12-membered ligands which are oxidized to Mn^{3+} species. The proton relaxivities of the bishydrated complexes are two times higher than those for monohydrated complexes and are comparable to those of commercial contrast agents based on Gd^{3+} complexes. Variable-temperature ^{17}O NMR data revealed that the water exchange varies from slow to intermediate or to extremely fast, depending on the ligand. High-pressure ^{17}O NMR measurements confirmed dissociative water exchange mechanism on complexes with CN = 7 and associative mechanism on complexes with CN = 6. Small endogenous bidentate anions (phosphate, citrate) are capable of replacing only one water molecule in the bishydrated complex with the 15-membered pentaaza ligand ($\mathbf{L^2}$), while in other cases the complex is slowly decomposed or no influence is observed.

Keywords:

Manganese(II) complexes, polyaza macrocycles, pyridine macrocycles, crystal structures, stability constants, dissociation kinetics, relaxometry, high-pressure ^{17}O NMR, NMRD, water exchange, Magnetic Resonance Imaging.

Abstrakt

Disertační práce je zaměřena na syntézu a studium manganatých komplexů jako alternativy ke komplexům gadolinitým, což jsou široce využívané kontrastní látky pro tomografii magnetické rezonance (Magnetic Resonance Imaging, MRI). V rámci nalezení vhodných manganatých komplexů jako potenciálních kontrastních látek pro MRI byly zkoumány tři strukturně rozdílné skupiny pentadentátních ligandů lišících se velikostí makrocyklické kavity, druhem donorových atomů a počtem pendantních ramen obsahující různé funkční skupiny. Z krystalových struktur bylo zjištěno, že Mn^{2+} iont má v těchto komplexech koordinační číslo 6 nebo 7, což umožňuje koordinaci jedné nebo dvou molekul vody. Přímá koordinace molekuly vody ovšem snižuje celkovou stabilitu komplexu a proto je termodynamická stability studovaných komplexů nižší než pro komplexy s polyaminokarboxyláty a stejně tak jejich disociace je mnohem rychlejší v porovnání s [Mn(nota)] nebo $[Mn(dota)]^{2-}$. Všechny studované manganaté komplexy jsou stálé vůči oxidaci vzdušným kyslíkem s výjimkou dvou komplexů s 12-člennými makrocykly, které jako jediné podléhají oxidaci za vzniku manganitých komplexů. Hodnoty relaxivity komplexů se dvěma koordinovanými molekulami vody jsou přibližně dvakrát vyšší než pro komplexy s jednou molekulou vody a zároveň jsou srovnatelné s relaxivitou komerčních kontrastních látek založených na gadolinitých komplexech. ^{17}O NMR měření při různých teplotách ukázalo, že rychlost výměny vody na zkoumaných komplexech je závislá na druhu ligandu – od velice pomalé, přes střední až po extrémně rychlou. Z výsledků ^{17}O NMR měření při vysokém tlaku byl potvrzen mechanismus výměny koordinované vody, který je disociativní pro komplexy s koordinačním číslem 7 a asociativní pro komplexy s koordinačním číslem 6. Malé bidentátní anionty přítomné v plazmě (fosfát, citrát) jsou schopny substituovat pouze jednu ze dvou koordinovaných molekul vody v komplexu s 15-členným pentaaza-makrocyklem ($\mathbf{L}^2$), zatímco v ostatních případech nemá přítomnost těchto aniontů na komplex žádný vliv nebo dochází k pozvolnému rozkladu.

Klíčová slova:

manganaté komplexy, polyaza makrocykly, pyridinové makrocykly, krystalové struktury, konstanty stability, disociační kinetika, relaxometrie, vysokotlaké ^{17}O NMR, NMRD, výměna vody, Magnetic Resonance Imaging.

Introduction

Magnetic Resonance Imaging (MRI) has become one of the most powerful diagnostic modalities widely used in modern clinical medicine. This non-invasive technique produces images of high spatial resolution and does not use ionizing radiation, enabling repeated *in vivo* investigation of dynamic processes.[1] The low sensitivity of this method can be improved by the administration of a contrast agent (CA) which provides not only better image resolution, but also functional information. Today, the majority of CAs are T_1-agents that reduce the longitudinal (T_1) relaxation time of water protons in body tissues resulting in positive contrast on T_1-weighted MR images. These compounds are based on paramagnetic ions (Gd^{3+}, Mn^{2+}) which have to be bound in stable complexes because in a free, non-complexed form they show significant *in vivo* toxicity.[2,3] Nowadays, most of the currently used T_1-agents are complexes of Gd^{3+} (7 unpaired electrons) and their solid structures, solutions, *in vitro* and *in vivo* properties have been studied extensively.[4,5,6]

The behavior of the paramagnetic complex in water solution has been described by the Solomon–Bloembergen–Morgan (SBM) theory of paramagnetic relaxation which relates the microscopic parameters of the CAs to their MRI efficiency (Fig. 1).[6] The effectiveness of a CA is expressed by its proton relaxivity (r_1) which is defined as the paramagnetic enhancement of the longitudinal relaxation rate ($1/T_1$) of the water protons in 1mM aqueous CA solution. Relaxivity has inner- and outer-sphere contributions. The inner-sphere relaxivity originates from the transfer of the paramagnetic relaxation effect to the bulk *via* the exchange of directly coordinated water molecule(s) to the paramagnetic ion. Such water protons quickly relax in the vicinity of the paramagnetic centre and this effect is expanded to the whole solution by exchange of the coordinated water molecule(s) with those from the bulk. This exchange is characterized by the water exchange rate, k_{ex} (residence time

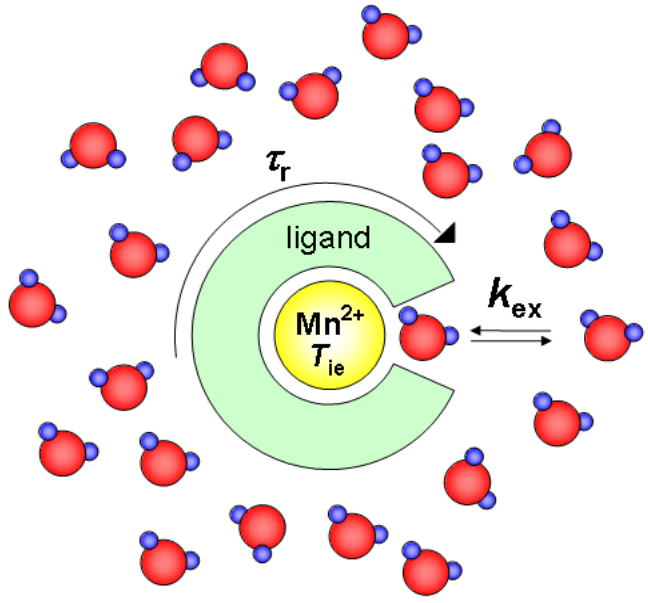

Fig. 1 Parameters influencing the relaxivity of a paramagnetic complex in aqueous solution

$t_M = 1/k_{ex}$). This parameter turned to be crucial for Gd^{3+} chelates since the exchange rate was found to be not sufficiently fast and many attempts have been made to accelerate water exchange. Another important parameter is the number of water molecules in the first coordination sphere (hydration number, *q*). Indeed, relaxivity is linearly proportional to the hydration number. Typically, there is only one coordinated water molecule in the complex, though some bishydrated complexes have been also described. However, the two water molecules in most of these bishydrated complexes are in adjacent position thus they are very easily substituted by small bidentate endogenous anions (carbonate, phosphate) under *in vivo* conditions. The loss of coordinated water molecules results in a distinct decrease of the CA efficiency. In addition, there are other microscopic parameters that govern inner-sphere relaxivity.[6] The transfer of the magnetic information between the paramagnetic ion and the water protons is controlled by the reorientation of the paramagnetic ion–proton vector, described by the rotational correlation time (t_R). In principle, the efficiency of this process is higher when the reorientation of the vector thus the molecular tumbling is slow. Another important parameter that influences relaxivity is electron spin relaxation (T_{ie}, i = 1, 2). These microscopic parameters can be optimized by appropriate ligand design to attain higher relaxivity. The currently used CAs have relaxivities in the range of 4–5 mM^{-1} s^{-1} which corresponds to ~ 5 % of the theoretical maximum value.[7] The main reasons for such low relaxivities of commercial CAs have been identified as the slow water exchange rate and the fast molecular motion. The outer-sphere relaxivity term arises from the random translational diffusion of water protons in the proximity of the paramagnetic ion. For small-molecular-weight chelates, it can contribute up to 50 % to the overall relaxivity, but this contribution can be hardly improved.

In comparison with Gd^{3+} chelates, much less attention has been devoted to transition metals that could also have a potential in MRI. Among them, Mn^{2+} with a high spin (5 unpaired electrons) and a slow electronic relaxation appears to be the best candidate. Additionally, the water exchange on Mn^{2+} complexes is sufficiently fast not to limit relaxivity while for Gd^{3+} chelates this could be a limiting factor.[4] The increasing number of publications with key words manganese and MRI can serve as a proof of the growing interest in this field (Fig. 2). In fact, Mn^{2+} played an important role in the history of magnetic resonance imaging since its aqua ion was the first CA proposed.[8]

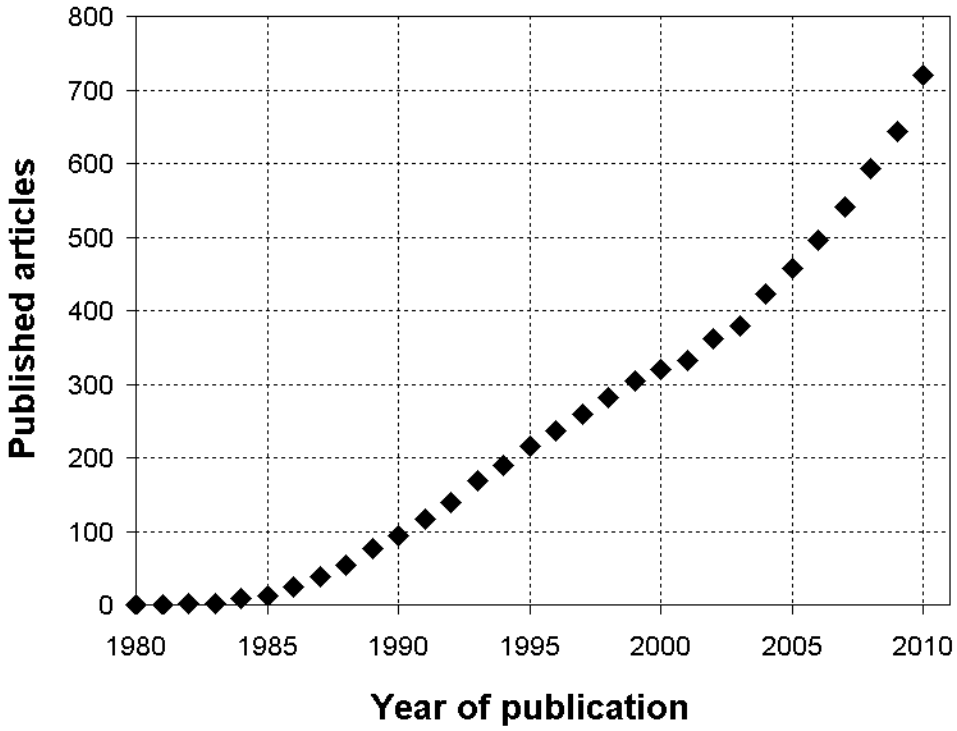

Fig. 2 Cumulative number of published articles obtained by a search in SciFinder database using keywords "manganese" and "MRI" performed on the 1st February 2011.

Moreover, Mn^{2+} is a biogenic element and in trace quantities is essential for normal development and body function. In particular, it is playing a key role as cofactor in a number of critical biological enzymes including manganese superoxide dismutase[9] – an important antioxidant defense in mitochondria, arginase[9] – the final enzyme in the urea cycle, or glutamine synthetase involved in neurotransmission (80% of manganese found in the brain).[10] Mn^{2+} has a very similar ionic radius to Ca^{2+} and it is handled in a similar manner to Ca^{2+} in many biological systems and processes. Therefore it exhibits a strong affinity to Ca^{2+} and Mg^{2+} binding sites in proteins[11] or nucleic acids[12] and it can be delivered across the Blood-Brain-Barrier into the brain from cerebral capillaries and/or cerebrospinal fluid or via the olfactory nerve.[3] Despite the important biological role of Mn^{2+}, large doses of this metal ion in humans are neurotoxic.[3] The overexposure to Mn^{2+} can lead to neurological disorders resulting in form of parkinsonism termed manganism which is likely caused by the damage of basal ganglia.[13] In addition, the accumulation of Mn^{2+} in the brain has been observed previously.[14]

During the last two decades, a specific field called "Manganese Enhanced Magnetic Resonance Imaging" (MEMRI)[15] has emerged on the basis of combining a strong relaxation effect of Mn^{2+} with its unique biology. This technique allows detailed visualization of brain structure, local brain or cardiac function and tracing of neuronal tracts. The main drawback

of this method is the toxicity of free $[Mn(H_2O)_6]^{2+}$, usually employed in the form of $MnCl_2$, at concentrations providing sufficient contrast and thus MEMRI is limited to small animal imaging.

To fulfill the function of CA, the Mn^{2+} chelate has to allow not only for direct coordination of water molecule(s) to the metal ion but thermodynamically and kinetically it must be sufficiently stable. In general, the thermodynamic stability of Mn^{2+} complexes is lower in comparison to Gd^{3+} analogues, which is related to the lower charge of the Mn^{2+} ion. It is also lower than for complexes with other transition metal ions due to the lack of ligand-field stabilization energy for high-spin d^5 electron configuration of Mn^{2+}. Besides the thermodynamic stability, the kinetic inertness is another important factor for safe *in vivo* application of CAs. The free toxic metal ion can be released from the complex by transmetallation with endogenous ions like Ca^{2+}, Zn^{2+} and Cu^{2+} or by proton-assisted dissociation resulting in the formation of free metal ion and free ligand – both toxic for the organism. In contrast to the large body of data describing the dissociation kinetics of Gd^{3+} chelates, there were no kinetic data available on Mn^{2+} complexes in the context of MRI. According to the *in vivo* study on $[Mn(dtpa)]^{3-}$ (ref.[14]), thermodynamically stable Mn^{2+} complexes were also supposed to be labile, but no experimental work has been done yet in a similar way as common for Gd^{3+} chelates.

As compared to the large number of commercially available Gd^{3+} chelates, there is only one example of a Mn^{2+} complex currently used in clinical practice. The compound $[Mn(dpdp)]^{4-}$ (Teslascan®, $dpdp^{6-}$ = *N,N'*-dipyridoxylethylenediamine-*N,N'*-diacetate-5,5'-bis(phosphate))[16] has found application in liver, kidney and heart imaging.[17,18] Surprisingly, this complex has no water molecule in the first coordination sphere and the observed *in vivo* relaxation effect arises mostly from the release of free Mn^{2+} from the complex. The slow release of free Mn^{2+} is ensured by the presence of the ligand which prevents toxicity that can be observed upon administration of $MnCl_2$.

In the context of MRI CAs, Mn^{2+} complexes of three classes of ligands have been previously investigated. The first class contains linear polyaminocarboxylates like EDTA[19,20] and its derivatives EDTA-$BOM_{1,2}$[21] and diPhEDTA[22] or derivatives of DPTA.[22,23,24] Macrocyclic ligands including derivatives of NOTA[25,26], DOTA[21,25,27,28] or AAZ3A[29] have been also described in the literature (Chart 1). The Mn^{2+} complexes of these ligands, originally mostly designed for Gd^{3+} complexation, have a maximum of one water molecule in the first coordination sphere except for the complexes with the third group of ligands based on polyaza- or polyaza-polyoxa-crown ethers (*e.g.* 15-aneN_5,[30] Me_2-15-pydieneN_5)[31] possessing

two inner-sphere water molecules. Recently, the Mn^{2+} complex of 1,7-DO2A[28] has been reported to have a remarkable relaxivity at 20 MHz, similar to that of $[Mn(H_2O)_6]^{2+}$.

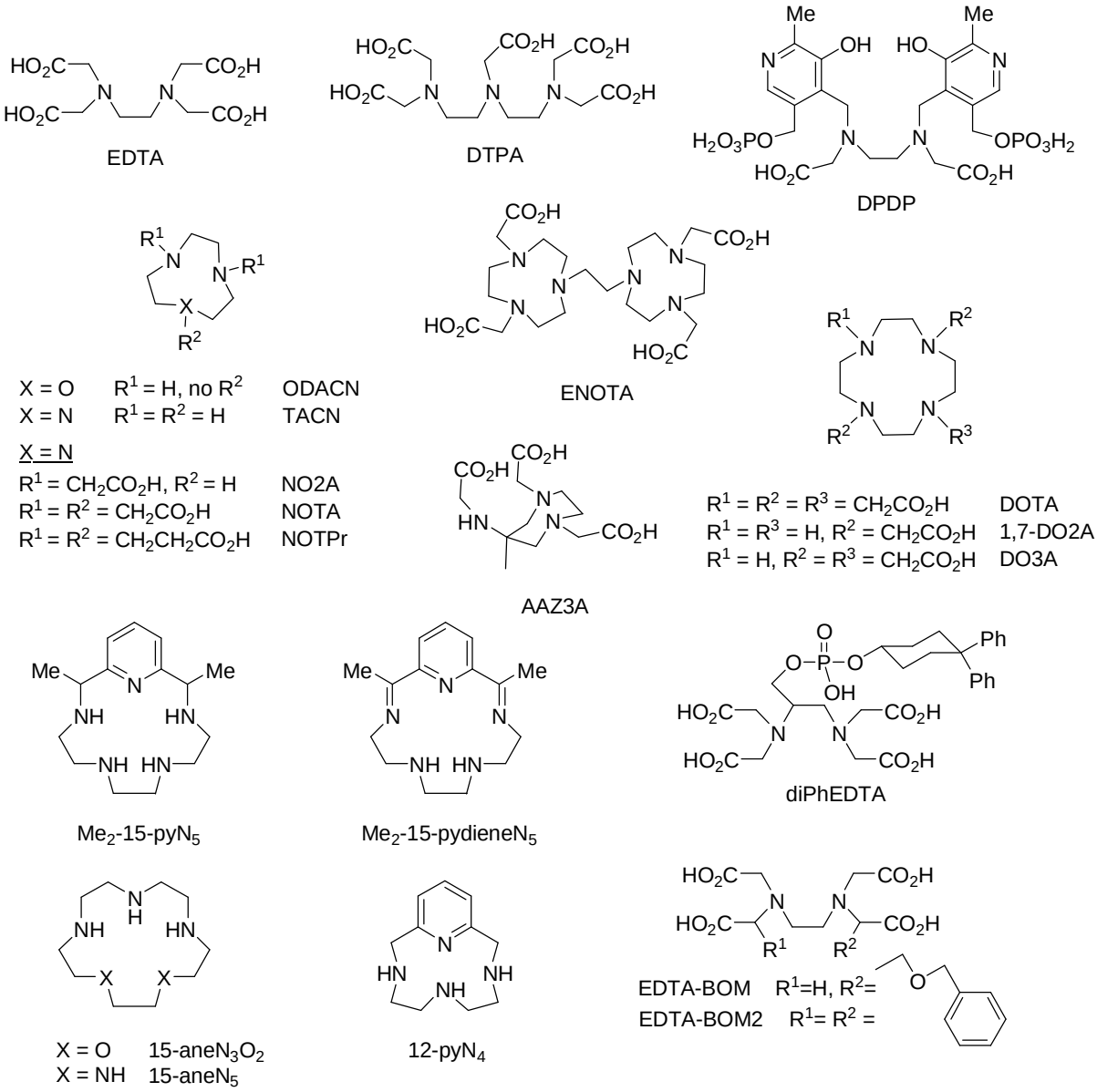

Chart 1 Structures of ligands discussed in the text

In summary, a Mn^{2+} complex must have a sufficient thermodynamic and kinetic stability and has to possess at least one coordination site for binding of an exchangeable water molecule to be effective as a T_1-CA for MRI. However, these requirements are contradictory since the decrease of number of donor atoms in the ligand enabling coordination of water molecule(s) might cause a dramatic decrease in stability. In addition, a sufficiently fast water exchange and slow molecular tumbling are also required, and the overall charge of the complex plays an important role in the pharmacokinetic behavior. To find the balance between these requirements in the ligand design remains a coordination chemistry challenge.

Objectives of the thesis

The structure of the ligand has a crucial influence on the properties of the Mn^{2+} complex. It determines the efficiency of the complex as an MRI CA as well as its stability required for a safe application. In the objective of creating stable Mn^{2+} complexes with good MRI efficiency, we have designed, synthesized and studied three classes of structurally different macrocyclic ligands (Chart 2). The usual coordination number in Mn^{2+} complexes is 6 or 7 and thus, pentadentate ligands have been chosen to provide at least one free coordination site for water binding in the complex.

The first class of ligands involves two 15-membered pyridine based macrocycles, **L^1** with two oxygen and three nitrogen, and **L^2** with five nitrogen donor atoms. The relatively rigid planar ligand structure is expected to lead to two water molecules in the Mn^{2+} complex coordinated in apical positions of the pentagonal-bipyramidal coordination sphere with overall CN = 7 for Mn^{2+}. The second class of ligands is based on 12-membered macrocycles containing also the pyridine ring and one pendant arm bearing a carboxylic acid (H**L^3**) or a phosphonic acid (H_2**L^4**) functional group. The macrocyclic scaffold has four nitrogens, the pendant arm provides one oxygen donor atom and the expected distorted octahedral sphere (CN of 6 for Mn^{2+}) should be completed with one water molecule. The last group of ligands is derived from 1-oxa-4,7-diazacyclononane. The 9-member macrocycle is modified by two pendant arms, both of them are bearing carboxylic acid (H_2**L^5**), phosphonic acid (H_4**L^6**), phosphinic acid (H_2**L^7**) or phenylphosphinic acid (H_2**L^8**) moieties. The two nitrogen and three oxygen donor atoms of the ligand would form a distorted octahedral spheres with CN of 6 for Mn^{2+}. The last free coordination site will be occupied by one water molecule leading to a monohydrated complex.

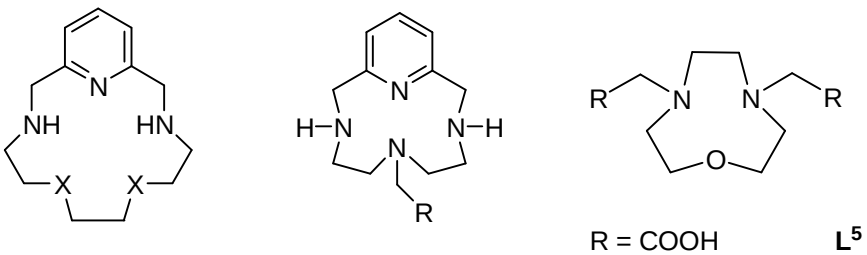

X = O **L^1**
X = NH **L^2**

R = COOH **L^3**
R = $P(O)(OH)_2$ **L^4**

R = COOH **L^5**
R = $P(O)(OH)_2$ **L^6**
R = P(O)(H)(OH) **L^7**
R = P(O)(Ph)(OH) **L^8**

Chart 2 Structures of studied ligands

The ligands and their Mn^{2+} complexes have been synthesized and fully characterized by different physico-chemical techniques with respect to their potential application as CAs for MRI. The structure of the ligands as well as of their complexes has been confirmed by X-

ray analysis. The protonation constants of the ligands and the thermodynamic stability constants of their complexes with Mn^{2+} and other selected metal ions have been determined by equilibrium potentiometry and pH NMR titration.

As few dissociation kinetic data have been published in the context of MRI, it led us to investigate the kinetic inertness of the Mn^{2+} complexes not only with the ligands mentioned above but also with NOTA and DOTA, two well-known ligands in biomedical applications. This first dissociation kinetics study of Mn^{2+} complexes, done under similar experimental conditions as common for open-chain Gd^{3+} chelates, has allowed the comparison of the complexes not only among each other but also with Gd^{3+} analogues. In particular, the data for $[Mn(nota)]^{-}$ and $[Mn(dota)]^{2-}$ dissociation might serve as a prime standard for comparison of further Mn^{2+} complexes.

Electrochemistry and UV-VIS measurements have been performed to characterize the stability toward oxidation to Mn^{3+} species which is widely observed in manganese chemistry. ^{17}O NMR and ^{1}H NMRD measurements have been used to assess the efficiency of the studied complexes as CAs by determining the microscopic parameters governing the relaxivity. Anion binding studies have been done to reveal the aptitude of the complexes towards substitution of water molecule(s) by small bidentate endogenous anions. All these experimental data on a large group of structurally different complexes should provide important insight into the relationships between the structural features of the ligand (cavity size, the choice of donor atoms and functional groups in the pendant arm(s)) and the relaxivity and stability of the Mn^{2+} complexes.

Experimental

Dry solvents were prepared by standard purification procedures,[32] distilled under argon and stored over 4Å molecular sieves in argon atmosphere: THF (Penta, distilled from Na,K/benzophenone), $CHCl_3$ (Penta, distilled from P_2O_5), MeOH (Penta, distilled from Na), DMF (Penta, distilled from P_2O_5), MeCN (Penta, distilled from P_2O_5), Toluene (Penta, distilled from K). Precursors have been prepared according to the literature procedures described previously – $\mathbf{L^1}$ and $\mathbf{L^2}$: Pyridine-2,6-dicarbaldehyde,[33] $\mathbf{L^2}$ **(**ref.[34] or slightly modified procedure, see Supporting Information in Appendix 1); H$\mathbf{L^3}$ and $H_2\mathbf{L^4}$: diethyl aminomethylphosphonate,[35] N-(4-toluenesupfonyl)aziridine,[36] ditosylated amine **1b** (4-diethoxyphosphorylmethyl-1,7-bis(4-toluenesulfonyl)-1,4,7-triazaheptane),[37] 1,7-bis(2-nitrophenylsulfonyl)-1,4,7-triazaheptane,[38] **1a** (4-((*tert*-butoxycarbonyl)methyl)-1,7-bis(2-nitrophenylsulfonyl)-1,4,7-triazaheptane),[38] protected cycle **2b**, 6-(diethoxyphosphoryl) methyl-3,9-bis(4-toluenesulfonyl)-3,6,9,15-tetraazabicyclo[9.3.1]pentadeca-1(15),11,13-triene,[37] and **2a**, 6-((*tert*-butoxycarbonyl) methyl)-3,9-bis(2-nitrophenylsulfonyl)-3,6,9,15-tetraazabicyclo[9.3.1]pentadecane-1(15),11,13-triene,[38] and 2,6-bis(bromomethyl) pyridine[39,40]; $H_2\mathbf{L^5}$–$H_2\mathbf{L^8}$: *N,N*'-bis(*p*-toluenesulfonyl)ethylenediamine,[34,41] *O,O*'-bis(*p*-toluene-sulfonyl)diethyleneglycol,[42] 4,7-bis(*p*-tolenesulfonyl)-1-oxa-4,7-diazacyclo nonane[43] and 1-oxa-4,7-diazacyclononane dihydrobromide (ODACN·2HBr).[44] Other solvents and chemicals including NOTA and DOTA were purchased from commercial sources and used as received.

NMR spectra were recorded at 25 °C on a Varian VNMRS300 spectrometer: ^{1}H 299.9 MHz, TMS (internal) δ = 0.0 ppm; ^{13}C 75.4 MHz, TMS (internal) δ = 0.0 ppm; $CHCl_3$ (internal) δ = 77.0 ppm; ^{31}P 121.4 MHz, H_3PO_4 (external) δ = 0.0 ppm or a Bruker Avance 500 MHz spectrometer: ^{1}H 500.1 MHz, TMS (internal) δ = 0.0 ppm; ^{13}C 125.8 MHz, TMS (internal) δ = 0.0 ppm; $CHCl_3$ (internal) δ = 77.0 ppm; ^{31}P 202.5 MHz, H_3PO_4 (external) δ = 0.0 ppm . Multiplicity of the signals is indicated as follows: s – singlet, d – doublet, t – triplet, q – quartet, m – multiplet, br – broad. Deuterated solvent $CDCl_3$ (99.8 % D) and D_2O (99.9 % D) from Chemtrade was used as received. Mass spectra were measured on a Bruker spectrometer ESQUIRE 3000 equipped with an electro-spray ion source and ion-trap detector in positive/negative mode and on an Autoflex instrument (Bruker Daltonics, Bremen, Germany) using MALDI-TOF ionisation/detection technique. For thin layer chromatography, Merck aluminum foils with silica gel 60 F254 impregnated with a fluorescent dye were used.

Elemental analyses were done at the Institute of Macromolecular Chemistry (Academy of Science of the Czech Republic, Prague).

Synthesis

3,12,18-triaza-6,9-dioxabicyclo[12.3.1]octadeca-1(18),14,16-triene (L^1)[45,46]

Pyridine-2,6-dicarbaldehyde (1.50 g, 11.1 mmol) and $MnCl_2 \cdot 4H_2O$ (2.18 g, 11.0 mmol) were dissolved in dry MeOH (150 ml). The solution of 1,8-diamino-3,6-dioxaoctane (1.66 g, 11.2 mmol) in dry MeOH (25 ml) was added drop-wise over 15 min. The yellow reaction mixture was heated for 2 h at 60 °C and became light brown. After cooling to 0 °C, $NaBH_4$ (5.61 g, 148.3 mmol) was added portion-wise. The solution was left stirring overnight at RT. Water (50 ml) was slowly added inducing precipitation of $Mn(OH)_2$ (which started to oxidize) and this suspension was stirred at RT for 1 h. MeOH was removed *in vacuo* and the remaining aqueous phase was extracted with CH_2Cl_2 (3×50 ml). The organic layer was dried with anhydrous sodium sulfate and the solvent was evaporated under reduced pressure. The crude product was purified by column chromatography (SiO_2, EtOH:NH_3(aq.) 20:1, R_f = 0.3) and dried *in vacuo* at 50 °C to obtain a yellowish oil (2.06 g, 74 % based on pyridine-2,6-dicarbaldehyde).

NMR ($CDCl_3$): ^{1}H δ 2.65 (br s, 2H, N*H*); 2.75 (m, 4H, OCH_2CH_2N); 3.51 (s, 4H, OCH_2CH_2O); 3.58 (m, 4H, OCH_2CH_2N); 3.81 (s, 4H, NCH_2py); 6.90 (d, 2H, C*H* arom., $^3J_{HH}$ = 7.8 Hz); 7.42 (t, 1H, CH arom., $^3J_{HH}$ = 7.8 Hz); $^{13}C\{^1H\}$ δ 49.0 (s, 2C, CH_2-N); 53.2 (s, 2C, CH_2-N); 69.5 (s, 2C, CH_2-O); 70.1 (s, 2C, CH_2-O); 120.4 (s, 2C, *C*H arom.); 136.9 (s, 1C, *C*H arom.); 156.9 (s, 2C, *C*-CH_2); MS *m/z* (+): 252.0 [$(L+H)^+$, calcd. 251.2]; 274.0 [$(L+Na)^+$, calcd. 274.2]; elemental analysis for $C_{13}H_{21}N_3O_2 \cdot C_2H_5OH \cdot 3H_2O$ found (calculated) C 50.86 (51.26); H 8.11 (9.46); N 11.68 (11.96).

6-carboxymethyl-3,6,9,15-tetraazabicyclo[9.3.1]pentadeca-1(15),11,13-triene (HL^3)

The protecting nosyl groups of **2a** were removed according to the literature procedure.[38] The solution of *tert*-butyle ester of unprotected cycle (1.54 g, 4.81 mmol) in 100 ml of dichlormethane was cooled to 0 °C in water-ice bath and trifluoroacetic acid (25 ml, 336 mmol) was added drop-wise. The solution was stirred at room temperature for 12h. Precipitated impurities were filtered off on glass frit S4 and the solvent with excess of trifluoroacetic acid were removed under reduced pressure. The residue was purified by flash silica gel chromatography (EtOH:NH_3 aq. 25% 10:1 to 1:1) and then cation exchange column (Dowex 50, H^+-form, 100 ml, elution with 15% HCl) and anion exchange column

(Dowex 1x8, OH^--form, 150 ml, elution with 15% HCl). Desire compound was obtained after evaporation of the MeOH solution as a yellow solid in form of dihydrochloride (0.55 g, 34% yield).

NMR (D_2O+DCl): ^1H δ 3.14 (t, 4H, NC*H*$_2$CH$_2$NH, $^3J_{HH}$ = 5.4 Hz); 3.30 (t, 4H, NCH$_2$C*H*$_2$NH, $^3J_{HH}$ = 5.4 Hz); 3.78 (s, 2H, C*H*$_2$-C(O)); 4.69 (s, 4H, NC*H*$_2$-py); 7.50 (d, 1H, C*H* arom., $^3J_{HH}$ = 8.1 Hz); 7.99 (t, 2H, C*H* arom., $^3J_{HH}$ = 8.1 Hz); $^{13}C\{^1H\}$ δ 48.8 (s, 2C, CH_2); 51.7 (s, 2C, CH_2); 55.3 (s, 2C, CH_2); 59.7 (s, 1C, CH_2); 124.7 (s, 2C, CH arom.); 142.2 (s, 1C, CH arom.); 151.3 (s, 2C, C arom.); 177.4 (s, 1C, COOH); MS *m/z* (+): 264.8 [$(L+H)^+$, calcd. 265.2]; 529.1 [$(2L+H)^+$, calcd.529.3].

6-dihydroxyphosphorylmethyl-3,6,9,15-tetraazabicyclo[9.3.1]pentadeca-1(15),11,13-triene (H_2L^4)

The solution of ditosylated cycle **2b** (6.98 g, 10.5 mmol) dissolved in 96% H_2SO_4 (70 ml) was divided into 20ml tubes that each contained 1 ml of this solution. Each tube was heated to 70 °C then put in the 160 °C oil bath for exactly 90 s and leave to cool to room temperature in air. The solutions from all tubes were collected in 600ml beaker and cooled with water-ice bath to 0 °C. The product precipitated as a hydrosulfate during addition of diethylether (350 ml). The solid was decanted with diethylether (2x200 ml), dissolved in 10% NH_3 (100 ml) and evaporated to dryness under reduced pressure. The residue was suspended in MeOH (25 ml), undissolved solid was filtered off on glass frite S3 and extracted with MeOH (3x10ml). Collected filtrates were evaporated under reduced pressure and the crude product was purified first on cation exchange column (Dowex 50, H^+-form, 120 ml, elution with 15% HCl) and then on anion exchange column (Dowex 1x8, OH^--form, 150 ml, elution with 15% HCl). The brown-yellow impurities were removed by 1h reflux in water (50ml) with activated charcoal. Pure product was obtained after evaporation of the MeOH solution as a slightly yellow solid in form of dihydrochloride (2.81g, 72% yield).

NMR (D_2O+DCl): ^1H δ 3.06 (t, 4H, NC*H*$_2$CH$_2$NH, $^3J_{HH}$ = 5.2 Hz); 3.21 (d, 2H, C*H*$_2$-P, $^2J_{PH}$ = 10.5 Hz); 3.34 (m, 4H, NCH$_2$C*H*$_2$NH); 4.68 (s, 4H, NC*H*$_2$-py); 7.49 (d, 1H, C*H* arom., $^3J_{HH}$ = 7.5 Hz); 7.99 (t, 2H, C*H* arom., $^3J_{HH}$ = 7.5 Hz); $^{13}C\{^1H\}$ δ 48.5 (s, 2C, CH_2); 52.3 (s, 2C, CH_2); 53.9 (d, 1C, CH_2, $^1J_{PC}$ = 151 Hz); 54.9 (s, 2C, CH_2); 124.8 (s, 2C, CH arom.); 142.4 (s, 1C, CH arom.); 151.3 (s, 2C, C arom.); $^{31}P\{^1H\}$ δ 23.4 (s); MS *m/z* (+): 300.8 [$(L+H)^+$, calcd. 301.1]; 601.2 [$(2L+H)^+$, calcd. 601.3]; (–): 298.7 [$(L–H)^–$, calcd. 299.1]; 599.1 [$(2L–H)^–$, calcd. 599.3].

1-oxa-4,7-diazacyclononane-4,7-diacetic acid (H_2L^5)

The solution of ODACN·2HBr (5.00 g, 17.1 mmol) in 25 ml of water was adjusted by 10% aq. NaOH to pH 9–10. The mixture was heated to 80 °C and a solution of bromoacetic acid (5.94 g, 42.8 mmol, 2.5 eq.) in 25 ml of water was added during one hour. During addition of the alkylation agent, the pH was checked with a glass electrode and adjusted to pH 9–10 by adding 10% aq. NaOH solution. The reaction mixture was kept at this temperature overnight. The excess of solvent was removed *in vacuo*. The crude product was purified on a cation exchanger column (Dowex 50, H^+-cycle, 500 ml, elution with 5% aq. NH_3) and then on an anion exchanger column (Dowex 1x8, OH^--cycle, 150 ml, elution with 5% AcOH). After evaporation of the solvent under reduced pressure, the residue was several times evaporated in vacuo with a small volume of water and finally two times with 58% HBr. The pure product precipitated from a EtOH: 58% HBr – 1:1 solution during addition of Et_2O, it was filtered off on glass frit S4 and washed with Et_2O. The desired compound was obtained as white microcrystallic powder in form of $H_2\mathbf{L}^5\cdot 2HBr\cdot H_2O$ (5.40 g, 80% yield).

NMR (D_2O): ^1H δ 3.42 (t, 4H, NCH_2CH_2O, $^3J_{HH}$ = 5.2 Hz); 3.53 (s, 4H, NCH_2CH_2N); 3.95 (t, 4H, NCH_2CH_2O, $^3J_{HH}$ = 5.2 Hz); 4.06 (s, 4H, CH_2CO_2H); $^{13}C\{^1H\}$ δ 53.87 (s, 2C, NCH_2CH_2O); 56.42 (s, 2C, NCH_2CH_2N); 58.92 (s, 2C, NCH_2CH_2O); 67.92 (s, 2C, CH_2CO_2H); 173.18 (s, 2C, CO_2H); MS *m*/*z* (+): 246.8 [$(M+H)^+$, calcd. 247.1]; 268.7 [$(M+Na)^+$, calcd. 269.1]; *m*/*z* (–): 244.6 [$(M–H)^-$, calcd. 245.1]; TLC: *i*-PrOH:aq. NH_3:H_2O 7:3:3, R_f = 0.70; elemental analysis for $H_2\mathbf{L}^5\cdot 2HBr\cdot H_2O$, $C_{10}H_{22}Br_2N_2O_6$, M_r = 426.10, found (calculated): C 28.64 (28.19); H 5.18 (5.20); Br 36.90 (37.50); N 6.53 (6.57).

Tetraethyl 1-oxa-4,7-diazacyclononane-4,7-bis(methylene phosphonate) (Et_4L^6)

The solution of ODACN·2HBr (3.00 g, 10.3 mmol) in 10 ml of aq. NaOH solution (pH = 12) was extracted with $CHCl_3$ (3×10 ml). The organic layer was dried over anhydrous sodium sulfate and the solvent was evaporated under vacuum to afford a yellow oil of 1-oxa-4,7-diazacyclononane that was directly used in the further reaction. It was dissolved in 10 eq. of $P(OEt)_3$ (17 ml, 103 mmol) and paraformaldehyde (0.77 g, 25.8 mmol, 2.5 eq.) was added. The flask with the reaction mixture was closed with a plastic stopper and heated to 60 °C for 12 h. The unreacted paraformaldehyde was filtered off on a glass frit S3 and washed with a small amount of EtOH. The filtrate was purified on a cation exchanger column (Dowex 50, H^+-cycle, 300 ml, washed with 1.5 l of EtOH, 0.5 l of water followed by elution with 2.5% NH_3 in EtOH). The eluate was evaporated to dryness to afford a pale yellow oil (2.49 g, 60% yield).

NMR (D_2O): ^{1}H δ 1.28 (t, 12H, OCH_2CH_3, $^3J_{HH}$ = 7.2 Hz); 2.91 (s, 4H, NCH_2CH_2N); 2.99 (t, 4H, NCH_2CH_2O, $^3J_{HH}$ = 3.6 Hz); 3.15 (d, 4H, CH_2P, $^2J_{PH}$ = 9.9 Hz); 3.70 (t, 4H, NCH_2CH_2O, $^3J_{HH}$ = 3.6 Hz); 4.11 (dq, 8H, OCH_2CH_3); $^{13}C\{^1H\}$ δ 15.70 (s, 4C, OCH_2CH_3); 51.40 (d, 2C, PCH_2, $^1J_{PC}$ = 155.8 Hz); 54.87 (s, 2C, NCH_2CH_2N); 55.64 (s, 2C, NCH_2CH_2O); 64.21 (s, 4C, OCH_2CH_3); 70.38 (s, 2C, NCH_2CH_2O); $^{31}P\{^1H\}$ δ 27.72 (s, 2P); ^{31}P δ 27.72 (t, 2P, $^3J_{PH}$ = 7.7 Hz); MS *m*/*z* (+): 431.0 [$(M+H)^+$, calcd. 431.2].

1-oxa-4,7-diazacyclononane-4,7-bis(methylenephosphonic acid) (H_4L^6)

To a solution of $Et_4\mathbf{L^2}$ (1.80 g, 4.2 mmol) in 36 ml of dry MeCN, bromotrimethylsilane (12 ml, 91 mmol) was added dropwise slowly. The reaction mixture was stirred 24 h at RT in dark. The volatiles were removed under vacuum and the residue was two times evaporated with 50 ml of dry EtOH. After trituration of the residue in other 50 ml of dry EtOH, the crude product was obtained as a white powder and filtered off on a glass frit S4. It was dissolved in a minimum of water and purified on a cation exchanger column (Dowex 50, H^+-cycle, 250 ml, elution with water). The presence of the product in 20 ml fractions was detected by TLC (*i*-PrOH:aq. NH_3:H_2O 7:3:3, R_f = 0.25, detection with $Cu(OAc)_2$ aq. solution). The collected fractions containing the product were evaporated under reduced pressure and the residue was dissolved in a minimum of water. This solution was added dropwise to 30 ml of dry EtOH. The white microcrystalline product precipitated from the solution, it was filtered off on a glass frit S3, washed three times with a small amount of dry EtOH and dried *in vacuo* (0.60 g, 60% yield).

NMR (D_2O): ^{1}H δ 2.94 (d, 4H, CH_2P, $^2J_{PH}$ = 10.8 Hz); 3.21 (t, 4H, NCH_2CH_2O, $^3J_{HH}$ = 4.2 Hz); 3.23 (s, 4H, NCH_2CH_2N); 3.81 (t, 4H, NCH_2CH_2O, $^3J_{HH}$ = 4.2 Hz); $^{13}C\{^1H\}$ δ 50.50 (s, 2C, NCH_2CH_2O); 51,96 (d, 2C, PCH_2, $^1J_{PC}$ = 146.9 Hz); 52.69 (s, 2C, NCH_2CH_2N); 65.31 (s, 2C, NCH_2CH_2O); $^{31}P\{^1H\}$ δ 11.76 (s, 2P); ^{31}P δ 11.76 (t, 2P, $^2J_{PH}$ = 10.2 Hz); MS *m*/*z* (+): 319.1 [$(M+H)^+$, calcd. 319.1]; 341.2 [$(M+Na)^+$, calcd. 341.1]; 357.1 [$(M+K)^+$, calcd. 357.0]; *m*/*z* (–): 317.1 [$(M–H)^–$, calcd. 317.1]; 339.2 [$(M–2H+Na)^–$, calcd. 339.1].

1-oxa-4,7-diazacyclononane-4,7-bis(methylenephosphinic acid) (H_2L^7)

To a solution of ODACN·2HBr (3.00 g, 10.3 mmol) in 30 ml of water was added 50% aq. solution of H_3PO_2 (13.60 g, 103 mmol, 10 eq.). The reaction mixture was heated to 45 °C and paraformaldehyde (1.23 g, 41.2 mmol, 4 eq.) was added in a small portion during one hour. The mixture was stirred at 45 °C overnight and then concentrated under vacuum (not heated above 45 °C) to 1/5 of initial volume. This solution of the crude product was purified twice on a cation exchange column (Dowex 50, H^+-cycle, 100 ml, elution with water). The presence

of the product was monitored by TLC (EtOH:aq. NH_3 5:1, R_f = 0.4). The 50 ml fractions containing the desired product were collected and the solvent was evaporated. The pure ligand was dissolved in 20 ml of water and lyophilized to give a hydroscopic glassy solid (1.62 g, 55% yield).

NMR (D_2O): ^{1}H δ 3.49 (d, 4H, C*H*$_2$P, $^2J_{PH}$ = 9.9 Hz); 3.67 (t, 4H, NC*H*$_2$CH$_2$O, $^3J_{HH}$ = 7.2 Hz); 3.88 (s, 4H, NC*H*$_2$C*H*$_2$N); 4.07 (t, 4H, NCH$_2$C*H*$_2$O, $^3J_{HH}$ = 7.2 Hz); 7.29 (d, 2H, P*H*, $^1J_{PH}$ = 554.9 Hz); ^{13}C{^{1}H} (*t* = 40 °C): δ 52.8 (s, 2C, NCH$_2$CH$_2$O); 55.15 (s, 2C, NCH$_2$CH$_2$N); 56.4 (d, 2C, PCH$_2$, $^1J_{PC}$ = 87.3 Hz); 65.7 (s, 2C, NCH$_2$CH$_2$O); ^{31}P{^{1}H} δ 13.10 (br s, 2P); 12.71 (t, 2P, $^1J_{PD}$ = 85.0 Hz); ^{31}P δ 13.10 (d, 2P, $^1J_{PH}$ = 555.7 Hz); 12.71 (t, 2P, $^1J_{PD}$ = 85.0 Hz); MS *m/z* (+): [286.8 (M+H)$^+$, calcd. 287.1]; 308.7 [(M+Na)$^+$, calcd. 309.1]; 324.7 [(M+K)$^+$, calcd. 325.1]; *m/z* (–): [284.6 (M–H)$^-$, calcd. 285.1].

1-oxa-4,7-diazacyclononane-4,7-bis[methylene(phenyl)phosphinic acid] (H_2L^8)

ODACN·2HBr (3.00 g, 10.3 mmol) was dissolved in 30 ml of 1:1 aq. HCl. Phenylphosphinic acid (7.30 g, 51.5 mmol, 5 eq.) was added and the suspension was heated to 60 °C. Paraformaldehyde (1.90 g, 61.8 mmol, 6 eq.) was added in a small portion during one hour and the reaction mixture was stirred at 60 °C overnight. After cooling down to room temperature, the reaction mixture was purified on a cation exchanger column (Dowex 50, H^+-cycle, 300 ml, elution with 5 % aq. NH_3). The eluate was concentrated under reduced pressure and the residue was dissolved in a minimum of EtOH. After several days of standing at room temperature, the pure product precipitated from the solution as microcrystalline powder that was filtered off on a glass frit S3 and dried in dessiccator with P_4O_{10}. The desired compound was obtained in form of $(NH_4)H\mathbf{L}^8\cdot 2H_2O$ (3.18 g, 67% yield).

NMR (D_2O): ^{1}H δ 3.00 (bm, 12H); 3.64 (bm, 4H); 7.51–7.77 (m, 10H); ^{13}C{^{1}H} δ 52.23 (s, 2C, NCH$_2$CH$_2$O); 53.39 (s, 2C, NCH$_2$CH$_2$N); 55.30 (d, 2C, CH$_2$P, $^1J_{PC}$ = 104.1 Hz); 65.92 (s, 2C, NCH$_2$CH$_2$O); 128.75 (s, 4C, *C*H arom.); 131.11 (s, 4C, *C*H arom.); 131.86 (s, 2C, *C* arom. quart.); 135.20 (d, 2C, P*C* arom. quart., $^1J_{PC}$ = 127.8 Hz); ^{31}P{^{1}H} δ 23.91 (br s, 2P); ^{31}P δ 23.91 (s, 2P); MS *m/z* (+): 438.9 [(M+H)$^+$, calcd. 439.2]; 461.0 [(M+Na)$^+$, calcd. 461.1]; 477.5 [(M+K)$^+$, calcd. 477.1]; *m/z* (–): 436.8 [(M–H)$^-$, calcd. 437.1]; elemental analysis for $(NH_4)H\mathbf{L}^8\cdot 2H_2O$, $C_{20}H_{35}N_3O_7P_2$, M_r = 491.46, found (calculated): C 49.18 (48.88); H 7.32 (7.18); N 8.47 (8.55).

Potentiometric measurements

Potentiometric titrations were carried out to determine the protonation constants of the ligands and the stability constants of their complexes formed with selected metal ions at 1:1 and 1:2 metal-to-ligand molar ratios. Titrations were performed at 25.0±0.1 °C and at an ionic strength of I = 0.1 M (NMe_4Cl) using deionized water. The constant passage of argon saturated with the solvent vapor provided the inert atmosphere. The initial volume in the titration vessel was 5 ml. Titrations were performed with NMe_4OH solution (~0.2 M) and the ligand concentration in the titrated solutions was ~0.004 M. For each determination, three parallel titrations were carried out, one titration consisting of about 50 points. All equilibria were established quickly except the formation of Ga^{3+} complexes. In this case, the out-of-cell method using sealed glass ampoules was employed[47,48] and the waiting time for equilibrium varied from 2 days to 8 weeks.

The titrations were run in the $-\log[H^+]$ range from 2 to 12 (or until precipitation of the metal hydroxide) with an extra HCl added to the starting solution employing a PHM 240 pH-meter, a 2-ml ABU 901 automatic piston burette and a GK 2401B combined electrode (all Radiometer, Denmark).

The OPIUM software package was used for calculations.[49,50] The value of pK_w was 13.81. Stability constants of the M^{2+}–OH^- systems were taken from literature.[51] For more details about potentiometric titrations, see previous papers.[52] In the following text, pH will mean $-\log[H^+]$ and all the equilibrium constants are concentration constants.

Dissociation kinetics

The transmetalation of Mn**L**$^{\mathbf{2}}$, Mn**L**$^{\mathbf{3}}$, $[Mn(nota)]^-$ and $[Mn(dota)]^{2-}$ with Zn^{2+} was followed by monitoring the relaxivity at 0.5 MHz on a Stelar SMARTracer Fast Field Cycling relaxometer at constant temperature (25 °C) and ionic strength (0.1 M KCl). Other experimental conditions for Mn**L**$^{\mathbf{2}}$: c_{Mn2+} = 1 mM, 0.02 M MES buffer; MES = 2-(4-morpholino)ethanesulfonic acid), pH range 4.7–6.0, presence of 5, 10, 20, 30 and 50-fold excess of the exchanging Zn^{2+}; for Mn**L**$^{\mathbf{3}}$: c_{Mn2+} = 1 mM, 0.05 M *N*-methyl-piperazine; pH range 5.1–6.2 and the presence of 5, 10, 20 and 40-fold excess of Zn^{2+}; for $[Mn(nota)]^-$ and $[Mn(dota)]^{2-}$: c_{Mn} = 1 mM, 0.02 M *N*-methylpiperazine buffer, pH range 3.5–5.6 and the presence of 5, 10, 20, 30 and 50-fold excess of Zn^{2+}. Each sample was prepared by mixing 1 ml of a buffered $ZnCl_2$ solution of a given concentration with an appropriate amount of Mn^{2+} complex stock solution in a 10 mm NMR tube. The experiment time varied according to the pH and corresponded to at least four reaction half-times. Because of the long duration of

the experiments with $[Mn(nota)]^-$ and $[Mn(dota)]^{2-}$, the samples were stored in a thermostat at 25.0 °C between the relaxivity measurements. The pH was measured after each experiment. Parallel control measurements confirmed that the pH was stable during the experiment.

^{17}O NMR measurements

Variable-temperature ^{17}O NMR measurements of aqueous solutions of Mn^{2+} complexes (c_{MnL} = 5 mmol kg^{-1}, pH 8.0, in 0.1 M TRIS buffer; TRIS = tris(hydroxomethyl)amino methane) were performed on a Bruker Avance 500 MHz spectrometer (11.7 T, 67.8 MHz) in the temperature range 1–75 °C. The temperature was calculated according to previous calibration with ethylene glycol and MeOH.[53] Acidified water ($HClO_4$, pH = 3.3) was used as standard diamagnetic reference. The ^{17}O longitudinal (T_1) and transverse (T_2) relaxations times were obtained by the inversion-recovery pulse sequence[54] and Carl-Purcell-Meiboom-Gill spin-echo technique, respectively.[55] To eliminate the susceptibility corrections to the chemical shift[56] the sample was placed in a glass sphere fixed in a 10 mm NMR tube. To improve sensitivity, the amount of ^{17}O was enriched by adding $H_2{}^{17}O$ (10 % $H_2{}^{17}O$, CortecNet) to achieve approximately 1 % ^{17}O content in the sample.

The variable-pressure ^{17}O NMR measurements were performed on the same solutions on a Bruker ARX-400 spectrometer (9.4 T, 54.2 MHz) equipped with a homemade high-pressure probe head in the pressure range 1–200 MPa. The temperature (295 or 286 K) in the probe was regulated via a thermostatic ethanol bath. The sample was placed in a short 5mm NMR tube closed with special teflon cylinder and then mounted in the high-pressure probe. The acidified water ($HClO_4$, pH = 3.3) was used as a standard diamagnetic reference. The transverse (T_2) relaxations times were measured by the Carl-Purcell-Meiboom-Gill spin-echo technique.[55]

^{1}H NMRD measurements

The ^{1}H NMRD profiles of aqueous Mn^{2+} complex solutions (c_{Mn2+} = 5 mM, pH 8.0, 0.1 M TRIS buffer) were measured at 25 and 37 °C (for **L^{1}** and **L^{2}** at 50 and 65 °C as well) on a Stelar SMARTracer Fast Field Cycling NMR relaxometer (0.00024–0.24 T, 0.01–10 MHz ^{1}H Larmor frequency) and a Bruker WP80 NMR electromagnet adapted to variable-field measurements (0.47–1.88 T, 20–80 MHz ^{1}H Larmor frequency), and controlled by the SMARTracer PC-NMR console. The temperature was controlled by a VTC91 temperature control unit and maintained by a gas flow. The temperature was determined according to previous calibration with a Pt resistance temperature probe.

Ternary complex formation

Relaxometric titrations were carried out on a Stelar SMARTracer Fast Field Cycling NMR relaxometer at 0.5 MHz and 25 °C to assess ternary complex formation with small endogenous anions. A solution of the anion ($c_{phosphate} = c_{carbonate} = c_{citrate}$ = 100 mM) was added step-wise to 1 ml of the Mn^{2+} complex solution (c_{Mn} = 1 or 2 mM, 0.1 M TRIS buffer, pH 8.0) up to 50 or 100 equivalents of the anion.

Electrochemistry

Cyclic voltammetry experiments were carried out on an Eco-Tribo Polarograph (ECOTrend Plus, Prague) driven by PolarPro 5.1 software. A conventional electrochemical three-electrode type cell was used with an Ag/AgCl reference electrode, a platinum wire auxiliary electrode and a glassy carbon working electrode. The final potential values *vs.* normal hydrogen electrode (NHE) were obtained using the relation between the two reference electrodes: Ag/AgCl electrode (sat. KCl) *vs.* NHE = +198 mV. The measurements were performed in aqueous solutions in the presence of 0.05 M KCl (pH = 8.0 adjusted by KOH solution) as the supporting electrolyte, with a scan rate of 100 mV s^{-1} and at 10^{-3} M Mn^{2+} complex concentrations.

UV-VIS measurements

UV-Vis spectra of aqueous Mn^{2+} complex solutions (c_{Mn2+} = 5 mM, pH 8.0, 0.1 M TRIS buffer) were recorded on a Varian Cary 5000 spectrophotometer (230–700 nm, at 25 °C) at different time intervals. The sample was placed in 1 cm tempered double-wall cuvette and measured with a data interval of 2 nm.

Single crystal X-ray analysis

Single crystals suitable for X-ray analysis of the perchlorate salts of the free $\mathbf{L^1}$ and $\mathbf{L^2}$ were obtained by slow cooling of a saturated aqueous ligand solution, acidified by several drops of perchloric acid (conc. 65 %). The single crystals of their Mn^{2+} complexes were prepared by a slow vapor diffusion of Et_2O into the ethanol solution of the complex at 5 °C.

Single crystals of hydrobromide salt of $H_2\mathbf{L^4}$ were obtained by slow diffusion of acetone to the diluted aqueous HBr solution of the ligand. The crystals of $Mn\mathbf{L^3}$ were prepared by vapor diffusion of acetone to the deoxygenated aqueous solution of the Mn^{2+} complex (5 °C) which was prepared from solid $MnCl_2 \cdot 4H_2O$ and $H\mathbf{L^3} \cdot 2HCl$ (10% excess) by adjusting the pH with aq. NaOH to ~8. The single crystals of $Mn\mathbf{L^4}$ were grown during the vapor diffusion of

aceton to the deoxygenated MeOH solution of the complex which was prepared from solid $Mn(ClO_4)_2 \cdot 6H_2O$ and $H_2\mathbf{L}^4$ (10% excess) and appropriate amount of $LiOH \cdot H_2O$ (based on the ligand). Free form of $H_2\mathbf{L}^4$ without chloride ions was obtained after cation exchange column chromatography with starting dihydrochloride $H_2\mathbf{L}^4 \cdot 2HCl$.

Single crystals of $(NH_4)H\mathbf{L}^8 \cdot 2H_2O$ were obtained by a vapour diffusion of acetone into an aqueous solution. Single crystals of $[Mn(\mathbf{L}^8)]_2 \cdot 2H_2O$ were prepared by a slow evaporation of an aqueous solution.

The diffraction data were collected using a Nonius Kappa CCD diffractometer (Enraf-Nonius) at 150(1) K using Mo-*K*α radiation (λ = 0.71073 Å) and analysed using the HKL program package.[57] The structures were solved using direct methods and refined by full-matrix least-squares techniques (SIR92[58] and SHELXL97[59]). Scattering factors for neutral atoms were included in the SHELXL97 program.

In all structures, all non-hydrogen atoms were refined anisotropically. The hydrogen atoms were located in the electron density map, however, those belonging to the carbon atoms were fixed in the theoretical positions and those belonging to oxygen and nitrogen atoms were fixed in the original positions using the riding model with $U_{eq}(H) = 1.2\ U_{eq}(X)$.

Data evaluation

The analysis of the experimental ^{17}O NMR, ^{1}H NMRD and kinetic data was performed by the Micromath Scientist program (version 2.0, Salt Lake City, UT) using a least-square fitting procedure.[60]

Sample preparation for NMR measurements

The Mn^{2+} complexes have been prepared by mixing solutions of $MnCl_2$ or $Mn(ClO_4)_2$ and the ligand and slowly adjusting the pH to 8.0 by diluted KOH (or LiOH) or by use of 0.1 M TRIS buffer pH = 8.0. For complexes of $\mathbf{L}^1$ and $\mathbf{L}^2$ 10% ligand excess, of $H\mathbf{L}^3$ and $H_2\mathbf{L}^4$ 25% ligand excess and of $H_2\mathbf{L}^5$–$H_2\mathbf{L}^8$ twofold ligand excess was used. In case of $Mn\mathbf{L}^3$ and $Mn\mathbf{L}^4$, deoxygenated water was used for preparation of all solutions and the manipulations with samples were done under argon atmosphere preventing the oxidation to Mn^{3+} species by air oxygen.

The formation of the complexes was confirmed by measurement of the mass spectra. MALDI ionization technique was used for $Mn\mathbf{L}^1$ and $Mn\mathbf{L}^2$ providing complexes with coordinated anion coming from the matrix (HCCA = α-cyano-4-hydroxycinnamic acid). ESI ionization technique was employed for all other complexes.

$[Mn(\mathbf{L}^{1})]^{2+}$:

MS *m/z* (+): 341.1 $[(Mn\mathbf{L}^{1}Cl)^{+}$, calcd. 341.1].; 494.0 $[(Mn\mathbf{L}^{1}$ (CCA))$^{+}$, calcd. 494.1].

$[Mn(\mathbf{L}^{2})]^{2+}$:

MS *m/z* (+): 339.1 $[(Mn\mathbf{L}^{2}Cl)^{+}$, calcd. 339.1].; 492.1 $[(Mn\mathbf{L}^{2}$ (CCA))$^{+}$, calcd. 492.2].

$[Mn(\mathbf{L}^{3})]^{+}$:

MS *m/z* (+): 317.8 $[(Mn\mathbf{L}^{3})^{+}$, calcd. 318.1].

$[Mn(\mathbf{L}^{4})]$:

MS *m/z* (+): 353.8 $[(MnH\mathbf{L}^{4})^{+}$, calcd. 354.1].

$[Mn(\mathbf{L}^{5})]$:

MS *m/z* (+): 305.7 $[(Mn\mathbf{L}^{5}+Li)^{+}$, calcd. 306.1]; 605.1 $[(2Mn\mathbf{L}^{5}+Li)^{+}$, calcd. 605.1]; *m/z* (–): 333.6 $[(Mn\mathbf{L}^{5}+Cl)^{-}$, calcd. 334.0]; 543.9 $[(Mn\mathbf{L}^{5}+H\mathbf{L}^{5})^{-}$, calcd. 544.2].

$[Mn(\mathbf{L}^{6})]^{2-}$:

MS *m/z* (+): 377.7 $[(MnH_2\mathbf{L}^{6}+Li)^{+}$, calcd. 378.0]; *m/z* (–): 369.6 $[(MnH\mathbf{L}^{6})^{-}$, calcd. 370.0].

$[Mn(\mathbf{L}^{7})]$:

MS *m/z* (+): 345.7 $[(Mn\mathbf{L}^{7}+Li)^{+}$, calcd. 346.0]; 644.1 $[(Mn\mathbf{L}^{7}+\mathbf{L}^{7}+3Li)^{+}$, calcd. 644.1]; *m/z* (–): 373.9 $[(Mn\mathbf{L}^{7}+Cl)^{-}$, calcd. 374.0]; 624.0 $[(Mn\ \mathbf{L}^{7}+H\ \mathbf{L}^{7})^{-}$, calcd. 624.1].

$[Mn(\mathbf{L}^{8})]$:

MS *m/z* (+): 491.9 $[(Mn\mathbf{L}^{8}+H)^{+}$, calcd. 492.1]; 513.9 $[(Mn\mathbf{L}^{8}+Na)^{+}$, calcd. 514.1]; *m/z* (–): 525.8 $[(Mn\mathbf{L}^{8}+Cl)^{-}$, calcd. 526.0].

In the following text the short abbreviation MnL indicating the Mn^{2+} complex of appropriate ligand will be used instead of full formulas containing coordinated water molecule(s), charge or counter ions except the cases where the full formula is necessary.

Results and discussion

Synthesis

15-membered macrocycles

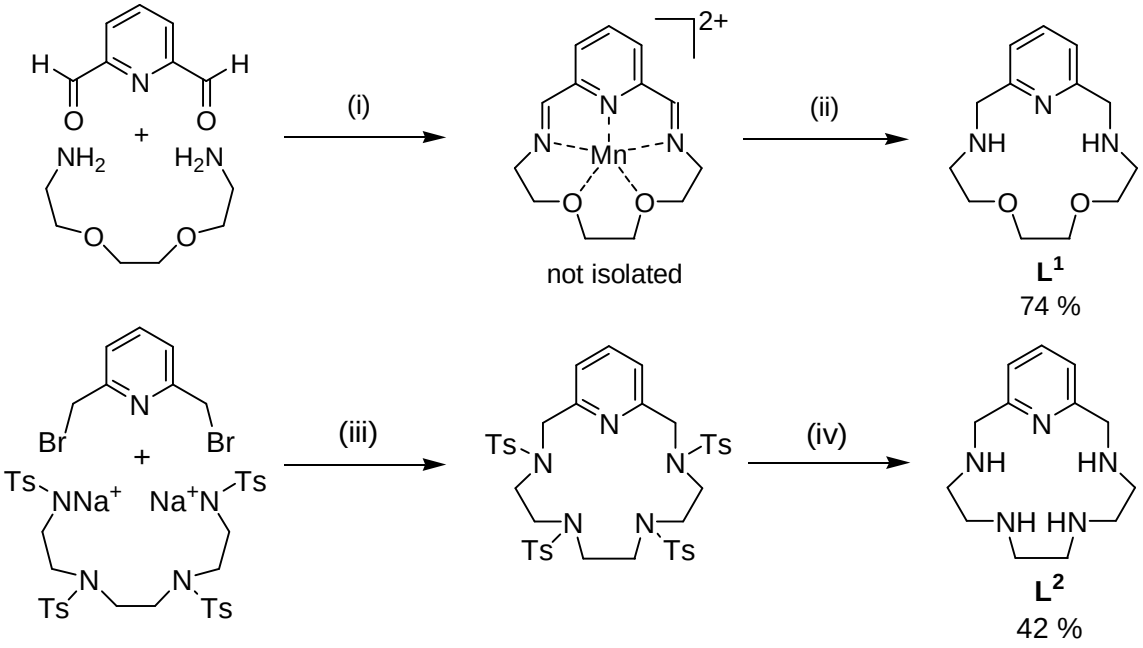

Scheme 1 Synthesis of ligand $\mathbf{L^1}$: (i) $MnCl_2$, MeOH, 60 °C, 2 h; (ii) 1. $NaBH_4$; 2. H_2O on air; and $\mathbf{L^2}$: (iii) DMF, 130 °C, 16h; (iv) 96% H_2SO_4, 100 °C, 1d.

The ligand $\mathbf{L^1}$ has been synthesized by template reaction on Mn^{2+}. The cyclization step proceeded *via* reaction of pyridine-2,6-dicarbaldehyde, prepared from commercially available pyridine-2,6-dicarboxylic acid[33] (Supporting Information in Appendix 1), with 1,8-diamino-3,6-dioxaoctane to form Mn^{2+} complex of the Schiff base which has been directly reduced with $NaBH_4$. The following hydrolysis of the hydride excess produced high basic conditions in which the manganese precipitated in the form of non-defined oxidized Mn^{3+} or Mn^{4+} species and thus, a simple demetalation occurred. The free ligand obtained was purified by silica gel column chromatography in an overall yield 74 %. Additional purification could be done by a high-vacuum distillation. The reaction conditions were similar to those previously described for the preparation of Mn^{2+} complexes with Schiff-bases derived from 2,6-diacetylpyridine and different amines or aminoethers.[46] This preparation produced higher yield and avoided the high-dilution technique employed for the synthesis of $\mathbf{L^1}$, by a template reaction on Mg^{2+}, published previously.[45] The attempt to prepare $\mathbf{L^2}$ by the same synthetic procedure failed, giving only a nonpurifiable reaction mixture. Therefore, the well-known slightly modified Atkins-Richman procedure using tosylate protecting groups has been

employed (see Supporting Information in Appendix 1). After column chromatography, **L**^{2} was obtained in form of light yellow solid in 42% overall yield.

12-membered macrocycles

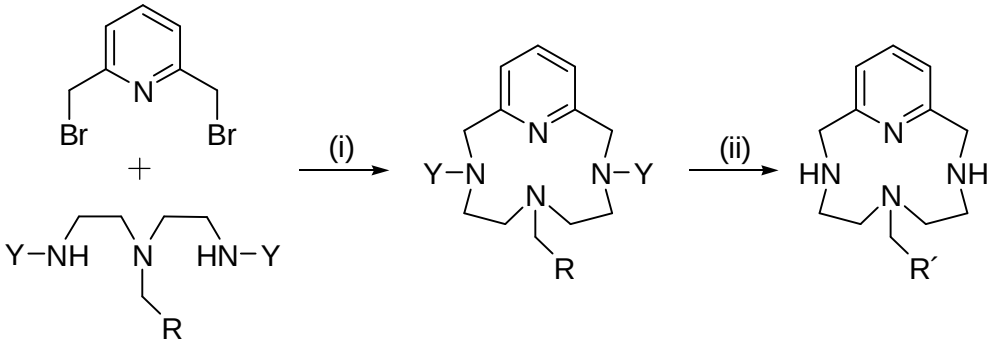

Y=Ns R=CO_2tBu R´=COOH	**1a**	**2a** 74 %	H**L**^{3} 34 %
Y=Ts R=PO_3Et_2 R´=PO_3H_2	**1b**	**2b** 78 %	H_2**L**^{4} 72 %

Ns = 2-nitrobenzenesulfonyl, Ts = 4-toluenesulfonyl

Scheme 2 Reaction scheme of synthesis of ligands H**L**^{3}: (i) K_2CO_3, MeCN, reflux 16h; (ii) (a) PhSH, Na_2CO_3, DMF, RT 12h; (b) TFA/CH_2Cl_2, RT 12h; and H_2**L**^{4} : (i) K_2CO_3, MeCN, reflux 16h; (ii) H_2SO_4 96%, Δ.

The synthesis of H**L**^{3} and H_2**L**^{4} has been already described elsewhere[37,38] but the compounds have been prepared only as intermediates and they were not isolated in free-acid forms. The procedures depicted in Scheme 2 employ common amino-protecting groups: 2-nitrobenzenesulfonyl (nosyl) for H**L**^{3} and 4-toluenesulfonyl (tosyl) for H_2**L**^{4}. The cyclization reaction of protected amines **1a** and **2a**, prepared by the literature procedures,[37,38] and 2,6-bis(bromomethyl)pyridine was done in dry MeCN using K_2CO_3 as a base[37] and gave protected ligands **2a** and **2b** in good yields (after purification by column chromatography). Deprotection of the cycles was the last but the most difficult step. The tosylate protecting groups in **2b** have been removed by heating the small volume (1ml) of the **2b** solution in concentrated sulfuric acid to 160 °C in an oil bath for very short period of time (90 s). Under such conditions a complete deprotection giving H_2**L**^{4} occurred without degradation of the phosphonate pendant arm (12-pyN_4 as a main product) which has been observed upon prolonged heating or higher temperatures. Aime et al. reported the same deprotection reaction[37] (3 g of **2b**, 15 ml of H_2SO_4) which was heated from 80 to 200 °C in 9 min., but in our hands the reaction under such conditions was not successful. The same reaction pathway has been used for the synthesis of H**L**^{3} but the appropriate conditions for the selective

deprotection in H_2SO_4 could not be found. The carboxylate pendant arm is much more sensitive to degradation (decarboxylation) than the phosphonate and even for lower temperatures and shorter reaction times used, the final mixture contained 12-pyN_4 and partially tosylated cycles with or without the pendant arm. These problems led to modification of the protecting group from tosyl to nosyl which allows moderate conditions of deprotection, typically RSH/DMF/base/RT. The nosyl groups in **2a** have been removed by reaction with thiophenole and Na_2CO_3 in DMF at room temperature[38] and the followed deesterification of *tert*-butyl ester with TFA in CH_2Cl_2 gave free form of H**L**^{3} (purified by silica gel and ion exchange column chromatography).

9-membered macrocycles

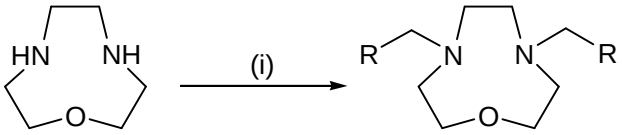

Ligand	Functional group in pendant arm	Reaction conditions	Yield
H_2**L**^{5}	R = COOH	(i) $BrCH_2COOH$, aq. NaOH (pH = 9–10), 80 °C, 12 h	80 %
H_4**L**^{6}	R = $P(O)(OH)_2$	(i) (a) $P(OEt)_3$, $(CH_2O)_n$, 60 °C, 12 h	60 %
		(b) 1. Me_3SiBr, MeCN, RT, 24 h 2. EtOH	60 %
H_2**L**^{7}	R = P(O)(H)(OH)	(i) 50 % aq. H_3PO_2, $(CH_2O)_n$, 45 °C, 12 h	55 %
H_2**L**^{8}	R = P(O)(Ph)(OH)	(i) $PhPO_2H_2$, $(CH_2O)_n$, 1:1 aq. HCl, 60 °C, 12 h	67 %

Scheme 3 Reaction scheme of the synthesis of ligands H_2**L**^{5}–H_2**L**^{8} with reaction conditions and yields

The synthesis of ligands H_2**L**^{5}–H_2**L**^{8} (Scheme 3) was based on the modification of 1-oxa-4,7-diazacyclononane (ODACN) which was prepared in form of dihydrobromide with 85% yield according to the literature procedure using tosylate protecting group and mixture of HBr:AcOH 1:1 as a deprotecting agent.[44] Two nitrogen atoms in ODACN enable their direct derivatization, resulting in required pentadentate ligands, which is easier than for TACN. In that case, the more difficult strategy of nitrogen atom protection has to be used to obtain similar pentadentate ligand with only two pendant arms.

H_2**L**^{5} was synthesized by alkylation of ODACN with excess of bromoacetic acid at pH 9–10 with almost complete conversion. This reaction has been published previously[61] and it is a well-known procedure how to modify macrocyclic amines with acetate pendant arms.

The two-step procedure of the synthesis of $H_4\mathbf{L}^6$ started by modified Mannich reaction preparing tetraethyl-ester $Et_4\mathbf{L}^6$ from the free base macrocycle, paraformaldehyde and excess of triethyl-phosphite (reactant and also solvent). Transformation of the dihydrobromide to the free base macrocycle provided better solubility in triethyl-phosphite and ensures the lack of bromide anions which induce the cleavage of the phosphonate ester group. The reaction progress was monitored by ^{31}P NMR. The excess of triethyl-phosphite was removed by column chromatography with cation exchange resin. The second step was hydrolysis of $Et_4\mathbf{L}^6$, but using of standard reagents like LiOH in EtOH/H_2O 1:1, 1M NaOH or HCl 1:1 failed. The conversion to tetrakis(trimethylsilyl) ester by reaction with bomotrimethylsilane had to be employed together with followed hydrolysis with EtOH resulting in free $H_4\mathbf{L}^6$ (an isolated yield of ~60 % based on $Et_4\mathbf{L}^6$). This ligand had been also prepared before but in very low yield.[62]

The two ligands $H_2\mathbf{L}^7$ and $H_2\mathbf{L}^8$ were prepared by Mannich reaction as well and they are the first amino(alkylphosphinic acids) to be described for small-ring oxaza macrocycles. The acidic conditions were ensured by excess of phosphinic acid (10 eq., $H_2\mathbf{L}^7$) or by using 1:1 aq. HCl solution ($H_2\mathbf{L}^8$). The reaction was accelerated by elevated temperature which was kept at 45 °C otherwise undesirable side-products with hydroxomethyl substituent in the pendant arm (instead of the P–H bond) and/or *N*-methylated derivatives appeared. Both ligands were purified by column chromatography on a strong cation exchange resin and eluted with water ($H_2\mathbf{L}^7$) or ammonia solution ($H_2\mathbf{L}^8$). Although the acidity/basicity of both compounds is very similar (*vide infra*), $H_2\mathbf{L}^8$ has a higher affinity to the resin mostly due to hydrophobic interactions between the phenyl rings of the phosphinic groups and the resin polymer. The use of ammonium solution during elution resulted in isolation of a monoammonium salt $(NH_4)H\mathbf{L}^8\cdot 2H_2O$, contrary to $H_2\mathbf{L}^7$ isolated in the form of free acid. This whole synthesis of ligands $H_2\mathbf{L}^5$–$H_2\mathbf{L}^8$ was done in cooperation with Mr. Miroslav Pniok and it was the main topic of his bachelor thesis.

Crystal structures

Crystal structures of free ligands

The structures of the investigated ligands and of some Mn^{2+} complexes have been confirmed by X-ray analysis. The ligands in free protonated form have been found in the crystal structures of $H_3\mathbf{L}^1(ClO_4)_3$, $H_4\mathbf{L}^2(ClO_4)_4\cdot H_2O$, $(H_4\mathbf{L}^4)(H_3\mathbf{L}^4)Br_3\cdot 0.5H_2O$ and $(NH_4)H\mathbf{L}^8\cdot 2H_2O$ (Fig. 3, 4 and 5). For interatomic distances, bond angles or other details conserning the X-ray data see Appendixes.

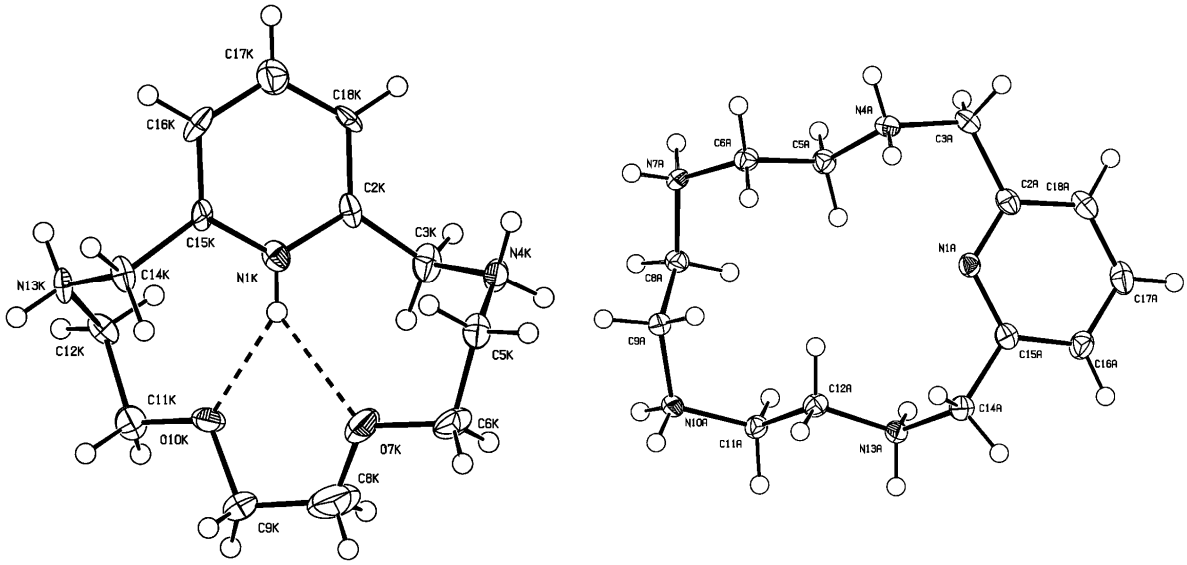

Fig. 3 Molecular structures of $(H_3\mathbf{L}^{\mathbf{1}})^{3+}$ (left) and $(H_4\mathbf{L}^{\mathbf{2}})^{4+}$ (right) ions found in the crystal structures of $H_3\mathbf{L}^{\mathbf{1}}(ClO_4)_3$ and $H_4\mathbf{L}^{\mathbf{2}}(ClO_4)_4{\cdot}H_2O$. The thermal ellipsoids are drawn with 50% probability.

Three independent ligand molecules adopting very close geometries were found in the structure of $H_3\mathbf{L}^{\mathbf{1}}(ClO_4)_3$ (Fig. 3). The molecules have a propeller-like shape, with a pseudo-C_2 symmetry axis. Both secondary amino groups as well as the pyridine nitrogen were found to be protonated. The protonation of the pyridine nitrogen atom is stabilized by two medium-strong hydrogen bonds involving the macrocycle oxygen atoms. The protonated secondary amino groups contribute to an extended hydrogen bond system involving oxygen atoms of the perchlorate counter ions.

In the crystal structure of $H_4\mathbf{L}^{\mathbf{2}}(ClO_4)_4{\cdot}H_2O$ (Fig. 3), two independent ligand molecules were found, adopting very similar conformations. All nitrogen atoms were protonated except the pyridine unit. An extended medium-strong hydrogen bond network is formed by protonated amino groups and perchlorate anions or solvate water molecules.

The crystal structure of $(H_4\mathbf{L}^{\mathbf{4}})(H_3\mathbf{L}^{\mathbf{4}})Br_3{\cdot}0.5H_2O$ (Fig. 4) contains two independent units with differently protonated ligand molecules and three bromide anions compensating the positive charge. These molecules have both secondary amino groups protonated in the macrocycle and differ in a number of protons attached to the phosphonate moiety in the pendant arm (one or two). The conformation of the macrocyclic parts in independent molecules is shovel-like because the position of the phosphonate moiety is turned above or away from the macrocycle. The phosphonate oxygen atoms are connected by a strong hydrogen bond ($d_{O\cdots O}$ ~2.44 and 2.49 Å) resulting in a centrosymmetric tetramer-like structure which is further stabilized by strong hydrogen bonds with neighbouring tetramers and weak interactions with bromide anions and water solvate molecules.

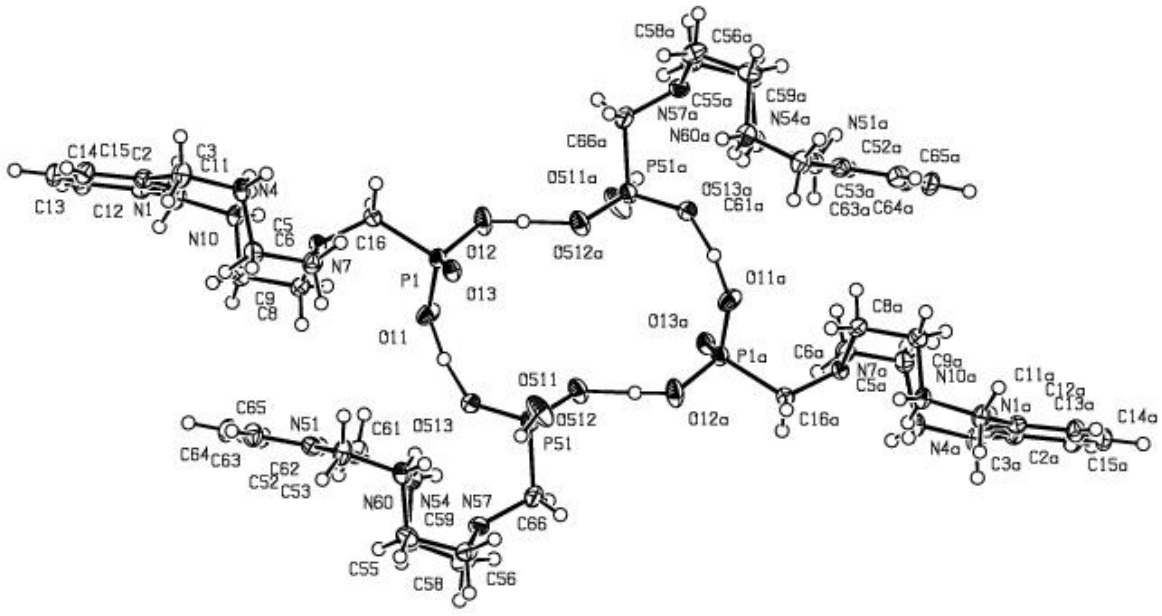

Fig. 4 Molecular structures of $\{(H_4\mathbf{L}^4)(H_3\mathbf{L}^4)\}_2^{6+}$ ion found in the crystal structure of $(H_4\mathbf{L}^4)(H_3\mathbf{L}^4)Br_3\cdot 0.5H_2O$. Hydrogen atoms attached to carbon atoms are omitted for the clarity. The thermal ellipsoids are drawn with 50% probability.

The ligand $H_2\mathbf{L}^8$ was isolated in the form of monoammonium salt $(NH_4)H\mathbf{L}^8\cdot 2H_2O$ (Fig. 5), the composition of which was confirmed by elemental analysis and X-ray diffraction study. Four formula units were presented in the independent unit without additional symmetry despite of very similar conformation of all ligand molecules. Both phosphinate pendant arms were deprotonated, the macrocyclic unit was monoprotonated on one nitrogen atom and the overall charge of the ligand molecule was compensated by the ammonium cation. The crown-like conformation of the macrocyclic unit is stabilized by an intramolecular hydrogen bond between the protonated amino group and the oxygen atom of the adjacent phosphinate. An extended intermolecular hydrogen-bond network between the protonated amino group and the phosphinate oxygen atoms of a neighbouring ligand molecule together with solvate water molecules and ammonium cations contributes to the structure stabilization.

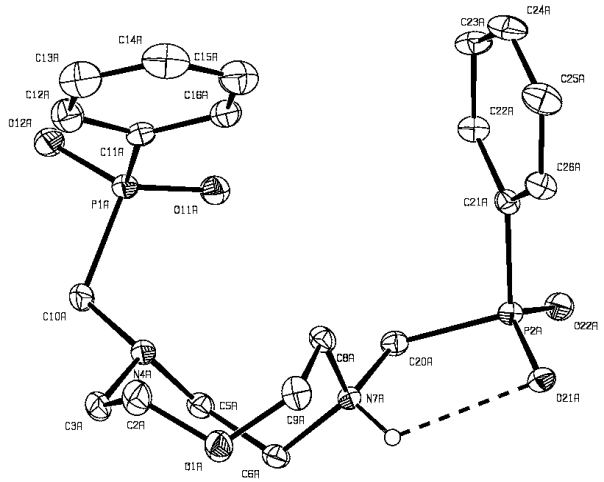

Fig. 5 Molecular structure of $(H\mathbf{L}^8)^-$ anion found in the crystal structure of $(NH_4)H\mathbf{L}^8\cdot 2H_2O$. The thermal ellipsoids are drawn with 50% probability.

Crystal structures of Mn^{2+} complexes

Despite many crystallization attempts, we could not obtain suitable crystals for X-ray analyses for all complexes studied. The experiments with $MnCl_2$ as a metal precursor showed a strong affinity of the chloride anion to Mn^{2+} and the chloride ion was coordinated instead of a water molecule even when a starting aqueous solution was used. In an attempt to prepare the desired complexes with the coordination of only water molecule(s), perchlorate was chosen as a counter-anion with low coordination ability (*e.g.* $Mn(ClO_4)_2$ as the starting salt). Unfortunately, these trials were not more successful. More details like interatomic distances or bond angles are given in Appendixes.

Mn^{2+} complexes of **L**^{1} and **L**^{2} have similar structures (Fig. 6). The central Mn^{2+} ion is coordinated in the centre of the planar macrocyclic cavity, with two other donor atoms in apical positions forming the pentagonal-bipyramidal coordination spheres. Both apical positions are occupied by chloride anions or one of them is substituted by one water molecule. Both these structurally different units were found in the structures of $[Mn(\mathbf{L}^{1})(Cl)_2]$ $[Mn(\mathbf{L}^{1})(H_2O)Cl]Cl{\cdot}1.5H_2O$, $[Mn(\mathbf{L}^{1})(H_2O)Cl](ClO_4)$ and $[Mn(\mathbf{L}^{2})(Cl)_2]$ $[Mn(\mathbf{L}^{2})(H_2O)Cl]_2Cl_2{\cdot}4H_2O$. All complex units have very similar pseudo-C_2 geometry of the macrocyclic part, with virtual two-fold axes laying on the Mn–N(pyridine) coordination bond. All compounds crystallized in the centrosymmetric unit except for the chiral $[Mn(\mathbf{L1})(H_2O)Cl](ClO_4)$ complex. The chirality of the chelate rings (starting from the pyridine nitrogen atom) was δλδλδ. The independent parts in other centrosymmetric units were chosen to adopt the same configuration. Other structural features were also very similar.

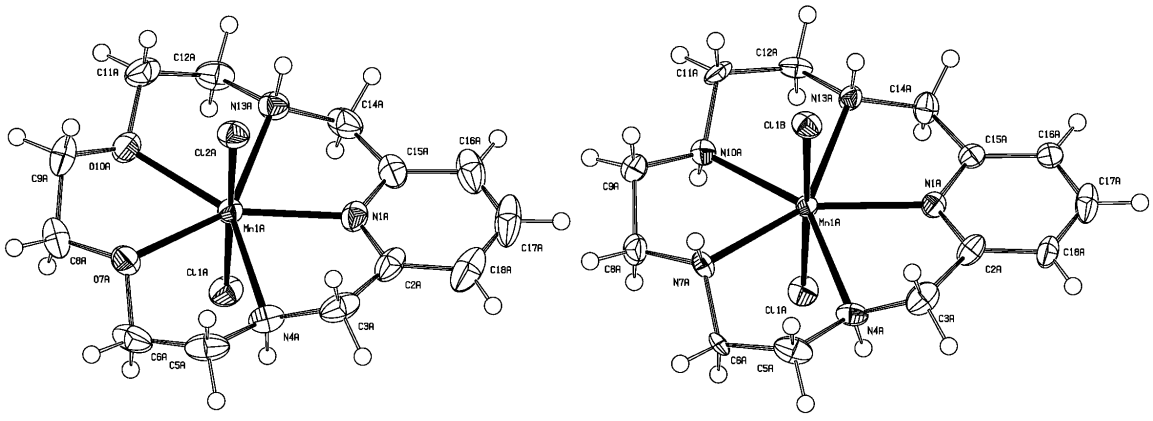

Fig. 6 The molecular structure of the $[Mn(\mathbf{L}^{1})(H_2O)Cl]^{+}$ (left) and $[Mn(\mathbf{L}^{2})(H_2O)Cl]^{+}$ (right) complex units found in the crystal structures of $[Mn(\mathbf{L}^{1})(Cl)_2][Mn(\mathbf{L}^{1})(H_2O)Cl]Cl{\cdot}1.5H_2O$ and $[Mn(\mathbf{L}^{2})(Cl)_2]$ $[Mn(\mathbf{L}^{2})(H_2O)Cl]_2Cl_2{\cdot}4H_2O$. The thermal ellipsoids are drawn with 50% probability.

In the crystal structure of $[Mn(\mathbf{L}^{3})Cl]{\cdot}1.5H_2O$ (Fig. 7), the Mn^{2+} ion is coordinated in a distorted octahedral fashion with CN = 6. The coordination sphere of Mn^{2+} comprises four

macrocyclic nitrogen atoms (with significantly shorter N(pyridine)–Mn coordination bond, ~2.20 Å), one carboxylate oxygen atom coming from the ligand and the last place is occupied by a chloride anion.

The independent unit found in the single-crystal of [Mn($\mathbf{L}^4$)]·1/6NaCl·1/3LiOH·9H_2O (Fig. 7) contains two complex species, which form two trimeric units symmetrical to the three-fold rotational axis.

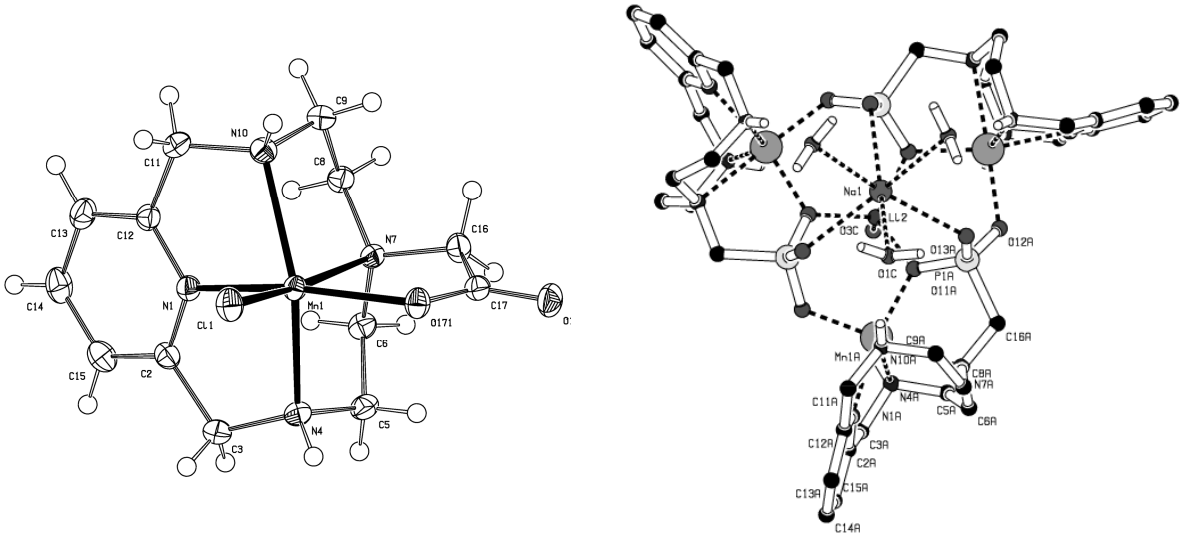

Fig. 7 The molecular structure of [Mn($\mathbf{L}^3$)Cl] (left) and the trimeric unit {Na(H_2O)$_3$[Mn($\mathbf{L}^4$)]$_3$Li(OH)} (right) found in the crystal structure of [Mn($\mathbf{L}^3$)Cl]·1.5H_2O and [Mn($\mathbf{L}^4$)]·1/6NaCl·1/3LiOH·9H_2O. For the trimeric unit, hydrogen atoms attached to the carbon atoms are omitted for the clarity reason. The thermal ellipsoids are drawn with 50% probability.

These trimers are templated either by sodium (laying on the axis and has 3 coordinated water molecules) and lithium ion (coordinated hydroxide ion probably) or by single lithium ion with apically coordinated hydroxide ion (probably). Mn^{2+} ion adopts distorted octahedral coordination sphere with CN = 6 composed by four nitrogen atoms and one phosphonate oxygen atom coming from the macrocyclic ligand. The last coordination site is occupied by a phosphonate oxygen atom from the neighbouring complex molecule. Despite the removal of chloride anions from $H_2\mathbf{L}^4$·2HCl by cation exchange chromatography, traces of NaCl were found in the crystals of Mn$\mathbf{L}^4$.

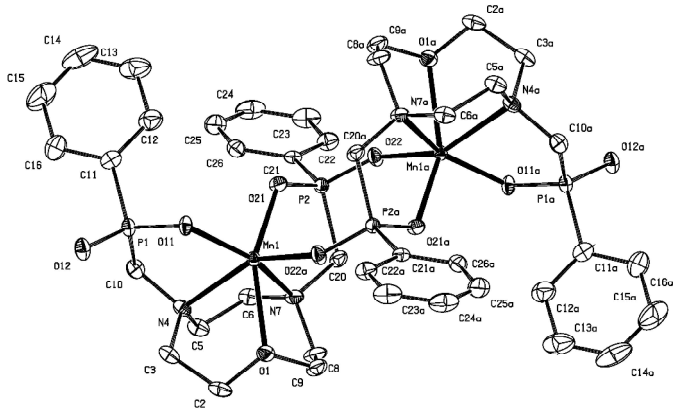

Fig. 8 Molecular structure of [Mn($\mathbf{L}^8$)]$_2$ dinuclear unit found in the crystal structure of [Mn($\mathbf{L}^8$)]$_2$·2H_2O. Hydrogen atoms attached to carbon atoms are omitted for the clarity. The thermal ellipsoids are drawn with 50% probability.

Only one example of a Mn^{2+} complex from the group of 9-membered ring ligands was successfully prepared for X-ray diffraction study. In the crystal structure of $[Mn(\mathbf{L}^{8})]_2 \cdot 2H_2O$ (Fig. 8), the Mn^{2+} ion is coordinated by three macrocycle donor atoms (N_2O) and two oxygen atoms (one of each phosphinate pendant arm). A phosphinate oxygen atom from the neighbouring complex molecule completes the coordination sphere, so a centrosymmetric dimer is formed with distorted octahedral spheres. The connection of the dimeric unit is provided by eight-membered $Mn(OPO)_2Mn$ entities which are common for phosphinate complexes and have been observed previously.[63]

The crystal structures confirmed CN = 7 for Mn^{2+} in Mn$\mathbf{L}^{1}$, Mn$\mathbf{L}^{2}$ adopting pentagonal-pyramidal coordination sphere. In Mn$\mathbf{L}^{3}$, Mn$\mathbf{L}^{4}$ and Mn$\mathbf{L}^{8}$, the Mn^{2+} ion was found in a distorted octahedral sphere with CN = 6. The coordinated chloride ions as well as the functional groups of neighbouring ligand molecule(s) found in the solid state are in aqueous solution replaced by water molecule(s) (*vide infra*). Thus, the structure of Mn$\mathbf{L}^{1}$ and Mn$\mathbf{L}^{2}$ allows the coordination of two water molecules in apical positions of the pentagonal bipyramide, whereas the octahedral arrangements of complexes Mn$\mathbf{L}^{3}$–Mn$\mathbf{L}^{8}$ provides only one water molecule in the first coordination sphere.

One complex was characterized with manganese in the oxidation state (III) (Fig. 9). The oxidation of the manganese(II) complex to manganese(III) one occurred during the slow crystallization process although the samples were kept under argon atmosphere, and resulted in the formation of deep red single-crystals of $[Mn(\mathbf{L}^{4})(OH)] \cdot 0.5LiCl \cdot 7H_2O$. The Mn^{3+} ion has also CN = 6 in a distorted octahedral coordination sphere similar to that of the Mn^{2+} analogue (four nitrogen and one phosphonate oxygen atoms) but the last site is occupied by a hydroxoanion which compensates the increased positive charge of Mn^{3+}. The trivalency of the central ion is evidenced by shortening of the coordination distances (shorter ionic radius of Mn^{3+}) in comparison with the corresponding Mn^{2+} complex.

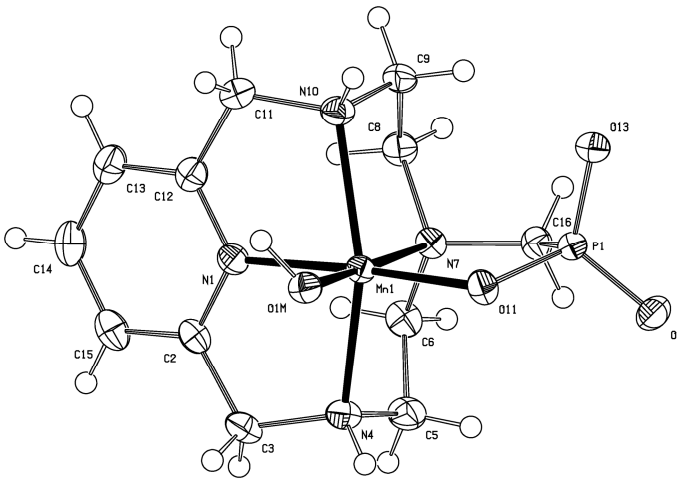

Fig. 9 The molecular structure of $[Mn(\mathbf{L}^{4})(OH)]$ found in the crystal structure of $[Mn(\mathbf{L}^{4})(OH)] \cdot 0.5LiCl \cdot 7H_2O$. The thermal ellipsoids are drawn with 50% probability.

Equilibrium studies

Protonation constants

Stepwise protonation constants of all investigated ligands have been determined by standard potentiometric titrations. The protonation constants obtained for $\mathbf{L^1}$–$H_2\mathbf{L^8}$ are listed in Table 1 and are compared to other structurally similar ligands (for the overall protonation constants with standard deviations see Supporting Information in Appendixes).

Table 1 Stepwise protonation constants[a] for ligands $\mathbf{L^1}$–$H_2\mathbf{L^8}$ compared to relevant ligands discussed in the text (25 °C, I = 0.1 M NMe_4Cl).

ligand	logK_{H1}	logK_{H2}	logK_{H3}	logK_{H4}	ref.
$\mathbf{L^1}$	8.82	7.80	–	–	this work
$\mathbf{L^2}$	9.40	8.54	5.28	–	this work
	9.43, 9.11	8.80, 8.82	5.28, 5.27	–	64,65
$H\mathbf{L^3}$	10.47 [10.53]	8.71 [9.10]	2.79 [2.82]	–	this work
$H_2\mathbf{L^4}$	11.84 [11.54]	9.64 [9.66]	6.23 [6.19]	0.99 [0.57]	this work
$H_2\mathbf{L^5}$	10.59	3.99	1.83	–	this work
	10.57	4.02	1.8	–	61
$H_4\mathbf{L^6}$	12.32	7.89	5.44	1.88	this work
$H_2\mathbf{L^7}$	8.42 [8.62]	1.39 [1.05]	[–1.6]	–	this work
$H_2\mathbf{L^8}$	9.23	1.85	–	–	this work
15-aneN_3O_2	9.51	8.47	2.30	–	66
15-aneN_5	10.31, 10.38	9.29, 9.51	5.93, 5.99	–	64,65
12-pyN_4	10.33	7.83	1.27	<1	67
ODACN	9.68	5.45	–	–	61
TACN	10.42	6.82	<1	–	68
NO2A	11.82	6.70	2.87	1.02	69

[a]Defined as $K_{Hi} = [H_iL]/[H^+]\times[H_{i-1}L]$ for i = 1–5 (charges were omitted for clarity).
The values in square brackets were calculated from $^1H/^{31}P$ NMR titration (no control of ionic strength).

In comparison to analogous non-pyridine macrocycles 15-aneN_3O_2 and 15-aneN_5, the basicity of $\mathbf{L^1}$ and $\mathbf{L^2}$ is lower, likely caused by the electron-withdrawing effect and/or by the increased rigidity of the macrocycle induced by the pyridine ring. The slightly lower values of the protonation constants for the oxygen-containing ligands can be related to the electron-withdrawing effect of the highly electronegative oxygen ($\mathbf{L^1}$ is less basic than $\mathbf{L^2}$, 15-aneN_3O_2 less than 15-aneN_5). The values measured for $\mathbf{L^2}$ are in good accordance with previously published data.[64,65]

Similar effect of the pyridine ring was observed for the 12-membered ligands H$\mathbf{L}^{3}$ and $H_2\mathbf{L}^{4}$. The increasing values of the first protonation constant, logK_{H1}, for 12-pyN_4 (no pendant arm), H$\mathbf{L}^{3}$ (one acetate arm) and $H_2\mathbf{L}^{4}$ (one phosphonate arm) can be accounted for by the presence of the functional group in the pendant arm. The increasing ligand basicity is in a good correlation with the positive inductive effect of the acetate and more importantly of the phosphonate pendant arm as observed previously for structurally related ligands.[63]

Similar influence of the functional group in the pendant arm was also observed for the ODACN based ligands $H_2\mathbf{L}^{5}$–$H_2\mathbf{L}^{8}$. The presence of the carboxylate and especially of the phosphonate pendant arm strongly increases the basicity of the ligand while the phosphinate or phenylphosphinate pendant arms induce an electron-withdrawing effect resulting in lower basicity of these two ligands. Similarly to the 15-membered ligands $\mathbf{L}^{1}$ and $\mathbf{L}^{2}$, an increase of basicity was observed when the oxygen atom was substituted by a nitrogen atom in the scaffold of $H_2\mathbf{L}^{5}$ (NO2A).

Protonation sequences

Recording the ^{1}H NMR spectra as a function of pH (pH-NMR titration) is well established method to assess the protonation sequences of polyaminocarboxylates, since the protonation of a basic site results in a deshielding of the resonance of the adjacent nonlabile protons in the ^{1}H NMR spectrum. For polyaminophosphonates/phosphinates, ^{31}P pH-NMR titration also can be performed to confirm the data from ^{1}H NMR. In that case, the upfield shift of ^{31}P resonance indicates the protonation of the nitrogen atom bearing the phosphorus-containing pendant arm which can be interpreted in terms of an intramolecular hydrogen bond formation between the protonated nitrogen atom and the deprotonated phosphonate/phosphinate. On the other hand, a downfield shift is caused by the protonation of the phosphorus-containing functional group.[70]

The protonation constants determined for $\mathbf{L}^{1}$ and $\mathbf{L}^{2}$ clearly correspond to the protonation of the secondary amino groups in the ligand scaffold while the protonation constant of the pyridine unit is too low to be detected under the experimental conditions. The recently published protonation sequence of $\mathbf{L}^{2}$ has confirmed our results.[71] Previous pH-NMR titrations of $H_2\mathbf{L}^{5}$ (ref.[61]) and $H_4\mathbf{L}^{6}$ (ref.[62]) revealed that the first protonation constant corresponds to the protonation of the macrocyclic nitrogen atom while the following two protonation steps occur on the carboxylate ($H_2\mathbf{L}^{5}$) or phosphonate ($H_4\mathbf{L}^{6}$) pendant arms. According to the upfield shift at very low pH in ^{31}P NMR, the log K_{H4} for $H_4\mathbf{L}^{6}$ represents the protonation of the second macrocyclic nitrogen atom.

pH-NMR titrations have been performed only for the ligands with uncertain protonation sequence (H**L**^{3}, H_2**L**^{4} and H_2**L**^{7}). The numbering or labeling of the hydrogen atoms of these ligands is depicted in Figs. 10 and 11. The results obtained for H**L**^{3} and H_2**L**^{4} are shown in Fig. 10 where the protonation constants calculated from potentiometry are also indicated (solid lines). The first protonation step occurs on the *tert*-amino group bearing the pendant arm (large downfield shift of almost all methylenic resonance in ^{1}H NMR, upfield shift in ^{31}P NMR). The second proton enters on the secondary amino group and simultaneously a proton transfer occurs from the *tert*- to the secondary amino group, to form species protonated only on the opposite secondary amino groups of the macrocycle that provide the lowest electrostatic repulsion. This proton transfer is more distinguishable for **L**^{4}, where it is confirmed by the complete recovery of the ^{31}P resonance at pH 8 while for **L**^{3} the first and second protonation steps appeared to be more overlapping and complex. The third protonation constants of both ligands (and log K_{H4} for H_2**L**^{4}) correspond to the protonation of the functional group in the pendant arm as confirmed by the largest downfield shift of the CH_2 resonance in the pendant arm in ^{1}H NMR and by the two downfield shifts in ^{31}P NMR.

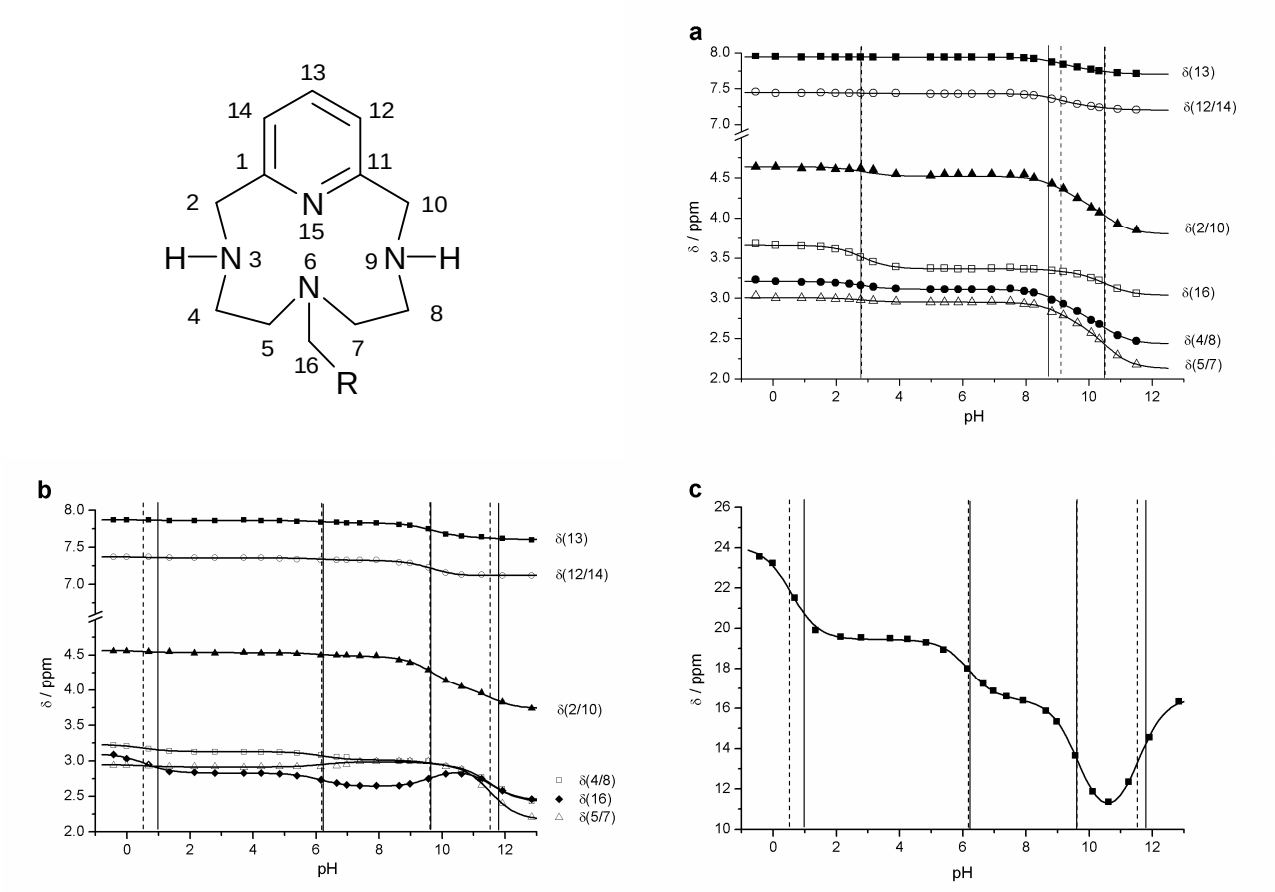

Fig. 10 Labeling of the macrocyclic ligands H_2**L**^{3} (R = COOH) and H_4**L**^{4} (R = PO_3H_2) together with the pH dependence of their ^{1}H NMR resonance: H**L**^{3}(a), H_2**L**^{4} (b) and the pH dependence of the ^{31}P NMR resonance for H_2**L**^{4} (c). The solid lines represent the logK_a values obtained from potentiometry, the dashed lines correspond to the values calculated from the NMR titration.

For $H_2\mathbf{L}^7$ and $H_2\mathbf{L}^8$, only two protonation constants have been determined under the experimental conditions exploited in potentiometry. In particular, the second protonation step was not straightforward to attribute. Therefore, ^1H and ^{31}P pH-NMR titration was performed for the more soluble $H_2\mathbf{L}^7$. The experimental titration data are displayed in Fig. 11 with those measured by potentiometry (solid lines). Based on the downfield shift of all CH_2 groups and on a very large upfield shift of the ^{31}P resonance between pH 7–10, the first protonation constant, log K_{H1}, was assigned to the protonation of the macrocyclic nitrogen atom, as was expected from the previous results on $H_2\mathbf{L}^5$ and $H_4\mathbf{L}^6$. Similar downfield shift of all ligand hydrogen atoms and an upfield shift of the ^{31}P resonance during the second protonation step between pH 0–2 pointed to the proton addition to the second macrocyclic nitrogen atom. The ring protonation occurs despite of the strong electrostatic repulsion between the two closely neighbouring positively charged ammonium ions. This surprising result is a consequence of the electron-withdrawing effect and the high acidity of the phosphinate acid moiety in the pendant arms.

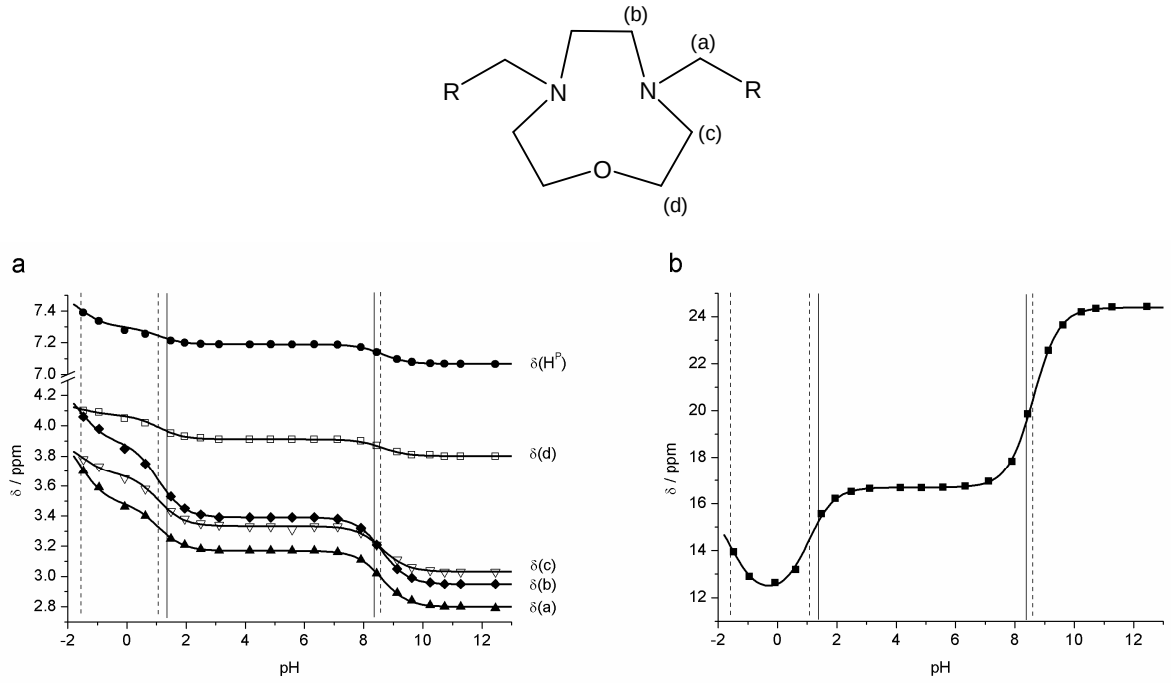

Fig. 11 Labeling of the macrocyclic ligand $H_2\mathbf{L}^7$ and NMR titration curves of its ^1H (a) and ^{31}P (b) individual resonances (no control of ionic strength). The vertical lines correspond to the protonation constants determined from potentiometry (solid lines) or from NMR titration (dashed lines).

Stability constants of studied complexes

The stability constants of complexes of all studied ligands with various metal ions have been determined by equilibrium potentiometry. Given the very large number of data which we obtained in the potentiometric titrations including all ligands and all different metal ions (Mg^{2+}, Ca^{2+}, Zn^{2+}, Cu^{2+}, Ga^{3+}, Co^{2+}, Cd^{2+}), here, for the sake of clarity, we list the stability

constants only for the Mn^{2+} complexes with $\mathbf{L^1}$–$H_2\mathbf{L^8}$ (Table 2; the full data sets are given in Supporting Information in Appendixes).

Table 2 Comparison of the stability constants[a] for Mn^{2+} complexes of studied ligands with those for other relevant ligands discussed in the text together with pMn[b] values and the percentage of free non-complexed Mn^{2+} for the systems with $c_{Mn2+} = c_{lig} = 5$mM or c_{Mn2+}=5mM, c_{lig}=10mM at pH 7.4.

ligand	log K_{ML}	log K_{HML}	log $K_{ML(OH)}$	% free Mn^{2+} c_{Mn2+}= c_{lig}=5mM	% free Mn^{2+} c_{Mn2+}=5mM, c_{lig}=10mM	pMn[b]	ref.
$\mathbf{L^1}$	7.18	–	–11.69	3.45	0.12	6.40	this work
$\mathbf{L^2}$	10.89	4.27	–11.52	0.12	3.8×10^{-4}	8.67	this work
$H\mathbf{L^3}$	11.54	4.95	–	0.37	1.3×10^{-3}	8.10	this work
$H_2\mathbf{L^4}$	14.06	5.35	–11.97	0.29	8.3×10^{-4}	8.30	this work
$H_2\mathbf{L^5}$	7.43[c]	–	–10.85	10.2	1.13	6.07	this work
$H_4\mathbf{L^6}$	10.61	6.32	–12.42	3.89	0.16	6.34	this work
$H_2\mathbf{L^7}$	4.30	–	–10.60[d]	28.6	9.48	6.01	this work
$H_2\mathbf{L^8}$	4.82	–	–10.84	36.3	15.2	6.00	this work
15-aneN_3O_2	6.63	–	–	24.2	6.74	6.01	66
15-aneN_5	10.55	3.66	–	2.66	7.23×10^{-2}	6.55	65
12-pyN_4	8.81	–	–	3.07	9.73×10^{-2}	6.46	67
ODACN	3.0[e]	–	–	97.2	93.9	6.00	61
TACN	5.8[f]	–	–	47.2	25.0	6.00	61
NO2A	11.56	–	–	0.42	1.7×10^{-3}	8.02	69
NOTA	16.30	2.87	–	7.77×10^{-3}	6.04×10^{-7}	11.47	this work
DOTA	19.89	4.26	2.99	3.60×10^{-4}	1.30×10^{-9}	14.14	27
DTPA	15.60	4.03	–	2.81×10^{-3}	1.28×10^{-7}	12.15	51
EDTA	13.88	–	–	4.40×10^{-3}	1.93×10^{-7}	11.97	51

[a] Defined as $K_{ML} = [ML]/[M]\times[L]$; $K_{ML(OH)i} = [ML(OH)_i]\times[H^+]/[ML(OH)_{i-1}]$; $K_{HML} = [HML]/[ML]\times[H^+]$.
[b] pMn = $-\log[Mn^{2+}_{free}]$ for pH = 7.4, $c_{Mn} = 10^{-6}$ M, $c_{lig} = 10^{-5}$ M. [c] log K_{ML2} = 2.37 was also determined. [d] log $K_{ML(OH)2}$ = –10.86 was also calculated. [e] log K_{ML2}=3.8 was also determined. [f] log K_{ML2}=3.6 was also determined.

Variation of the species including monoprotonated, monohydroxo- or dihydroxo- as well as dinuclear complexes has been observed in the systems studied (for distribution diagrams and more details see Appendixes). In accordance with the Irwing-Williams rule, the Cu^{2+} forms the most stable complexes along the transition metal ion series. On the other hand, Mn^{2+} chelates with d^5 high spin electron configuration and negligible ligand field stabilization energy exhibit the lowest thermodynamic stability among the transition metals complexes. The difference in the stability constants of Mn^{2+} and Cu^{2+} complexes of all ligands studied is between 7–9 orders of magnitude. Mg^{2+} and Ca^{2+} form weak complexes with all ligands showing no significant selectivity.

For a better comparison of the stability of Mn^{2+} complexes, the percentage of free Mn^{2+} in each system at physiological pH 7.4 (for $c_{Mn2+} = c_{lig}$ = 5 mM and for twofold ligand excess c_{Mn2+} = 5 mM, c_{lig} = 10 mM) and the pMn values (pMn = –log($c_{Mn2+free}$), for $c_{Mn2+} = 10^{-6}$ M, $c_{lig} = 10^{-5}$ M, pH = 7.4) were calculated and compared to those for structurally related complexes in Table 2. A high value of pMn and a low percentage of non-coordinated Mn^{2+} are indications of a good complex stability and the best values were found for the complexes of **L²**, H**L³** and H_2**L⁴**. These complexes are fully formed (>99%) at physiological pH (see Table 2, first column of % free Mn^{2+}) in a solution of equimolar ligand and metal concentration. Low pMn values and high percentage of non-complexed Mn^{2+} found for the other complexes imply their low stability. In such cases, the ligand excess can help to achieve complete complex formation. In particular, Mn**L⁷** and Mn**L⁸** have very low stability and the full complex formation was not achieved even for 2-fold ligand excess below pH 9. Therefore these two complexes were excluded from further studies where free Mn^{2+} can mislead the interpretation of the experiments (^{17}O NMR, NMRD).

It is evident that the polydentate aminocarboxylates (EDTA, DTPA, NOTA, DOTA) form much more stable complexes with Mn^{2+} than the ligands investigated. Nevertheless, the introduction of the pyridine ring into the ligand scaffold (**L¹** and **L²** vs. 15-aneN_3O_2 and 15-aneN_5) rigidifies the molecule and results in an increased complex stability. From the comparison of **L¹** and **L²**, H**L³** and NO2A or ODACN and TACN, one can conclude that the replacement of the oxygen(s) by nitrogen atom(s) leads to an increase of the ligand basicity which is reflected in an increased stability of the Mn^{2+} complex. The nature of the functional group in the pendant arm(s) of the 12- and 9-membered ligands affects the ligand basicity and has a crucial role in the coordination behavior of the ligand as well. The stability, not only of Mn^{2+} but also of other transition metal complexes, increases in the following order with the functional group: phosphinate< phenylphosphinate < acetate < phosphonate.

Dissociation kinetics

In addition to thermodynamic stability, high kinetic inertness is another condition required for safe *in vivo* application of a Mn^{2+} complex as CA. The *in vivo* toxicity of Mn^{2+} complexes is related to the release of free metal ion and free ligand as both are toxic for the organism. In general terms, the complex dissociation can proceed *via* a proton-assisted pathway or *via* metal-assisted exchange reactions with endogenously available ions such as Ca^{2+}, Zn^{2+} or Cu^{2+}.[6] In comparison to the large body of data reported for Gd^{3+} analogues, much less is known of Mn^{2+} complexes suitable for MRI applications, and in particular, the dissociation

kinetic aspects are essentially unexplored. Even Mn^{2+} complexes with high thermodynamic stability, like $[Mn(dpta)]^{3-}$, have been proven to be kinetically labile and did not prevent the accumulation of Mn^{2+} in the brain after administration of the agent.[14]

The dissociation kinetics of Gd^{3+} complexes was mainly investigated either in strongly acidic media (macrocyclic ligands like DOTA)[72,73] or in the presence of a high excess of competing metal ion (open-chain ligands like DTPA).[74,75] These non-physiological conditions allow to determine the dissociation rates, which would be extremely long to investigate under real physiological conditions, and to compare the kinetic inertness of different complexes studied in a similar way. The experimental conditions similar to those for the dissociation of Gd^{3+} complexes with open-chain ligands have been successfully employed also for macrocyclic Mn^{2+} complexes as they have not shown as extraordinary kinetic stability as macrocyclic Gd^{3+} complexes. Typically, the transmetallation reaction between the Mn^{2+} complex and the diamagnetic Zn^{2+} in 5–50-fold excess as the exchanging ion was monitored by relaxometry at pH 3.5–6.2. The relaxivity increase in time is the result of a release of free Mn^{2+} replaced by Zn^{2+} from the complex and, especially at low field, the difference in relaxivity between the complex with 0–2 inner sphere water molecules and $[Mn(H_2O)_6]^{2+}$ is large to allow for monitoring the reaction. Under such conditions, the dissociation of Mn**L**^{1}, Mn**L**^{4}, Mn**L**^{5} and Mn**L**^{6} were instantaneous (Mn**L**^{7} and Mn**L**^{8} were not tested due to their low thermodynamic stability), while above pH 6.2 the partial hydrolysis of Zn^{2+} prevented the measurement. Therefore we measured data only for Mn**L**^{2} and Mn**L**^{3}. In addition, Mn^{2+} complexes of NOTA and DOTA – two well known ligands in the context of MRI – have been studied as well.

The excess of exchanging metal ion ensures that the reaction rate is directly proportional to the total concentration of the complex, $[MnL]_{tot}$, and it is of pseudo-first order, equation (1), where k_{obs} is the pseudo-first order rate constant.

$$-\frac{d[\mathrm{MnL}]_{\mathrm{tot}}}{dt} = k_{\mathrm{obs}} \times [\mathrm{MnL}]_{\mathrm{tot}} \qquad (1)$$

Taking into account the presence of differently protonated complexes, whose stability constants have been determined from potentiometry, the general dissociation scheme involving proton-assisted as well as metal-assisted dissociation pathways is illustrated as shown in Scheme 4.

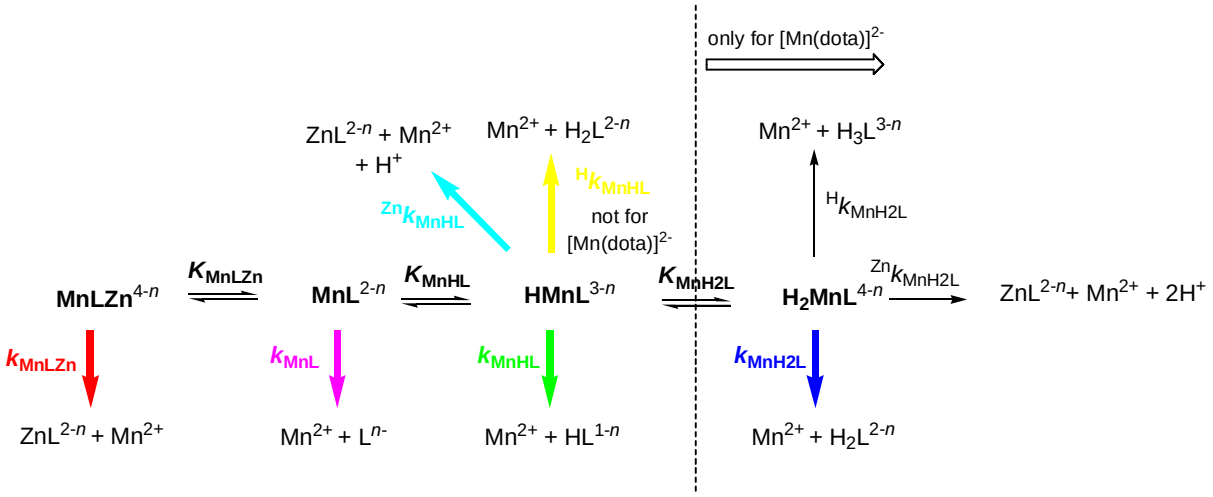

Scheme 4 Possible dissociation pathways for Mn**L**^{2} (n = 0), Mn**L**^{3} (n = 1), [Mn(nota)]$^{-}$ (n = 3) and [Mn(dota)]$^{2-}$ (n = 4). The pathways having a real contribution to the overall dissociation, as indicated by the fit of the observed rate constants, are represented in color (bold). Each color indicates the corresponding term in equations (4) or (5).

Considering the dissociation pathways in Scheme 4, the rate of the dissociation reaction is given by equation (2) (in the equations, the complex charges are omitted for clarity).

$$-\frac{d[\mathrm{MnL}]_{\mathrm{tot}}}{dt} = k_{\mathrm{MnL}}[\mathrm{MnL}] + k_{\mathrm{MnLZn}}[\mathrm{MnLZn}] + k_{\mathrm{MnHL}}[\mathrm{MnHL}] + {}^{\mathrm{Zn}}k_{\mathrm{MnHL}}[\mathrm{MnHL}][\mathrm{Zn}^{2+}] + {}^{\mathrm{H}}k_{\mathrm{MnHL}}[\mathrm{MnHL}][\mathrm{H}^{+}] + k_{\mathrm{MnH2L}}[\mathrm{MnH_2L}] + {}^{\mathrm{H}}k_{\mathrm{MnH2L}}[\mathrm{MnH_2L}][\mathrm{H}^{+}] + {}^{\mathrm{Zn}}k_{\mathrm{MnH2L}}[\mathrm{MnH_2L}][\mathrm{Zn}^{2+}] \quad (2)$$

Each term in equation (2) represents a dissociation pathway. The first term corresponds to the spontaneous dissociation of the non-protonated complex (pink color in Scheme 4), the second one to spontaneous dissociation of the dinuclear complex with Zn^{2+} (red), the third one to the spontaneous dissociation of the monoprotonated complex (green) and the next one to the zinc-assisted dissociation of the monoprotonated complex (light blue). The term representing the proton-assisted dissociation of the monoprotonated complex, ${}^{\mathrm{H}}k_{\mathrm{MnHL}}[\mathrm{MnHL}][\mathrm{H}^{+}]$ (yellow), applies only for [Mn(nota)]$^{-}$, Mn**L**^{2} and Mn**L**^{3} whereas the last three terms, related to the presence of diprotonated species (spontaneous, proton- and zinc-assisted dissociation), exist only for [Mn(dota)]$^{2-}$. The overall MnL concentration is the sum of the concentrations of different species and can be generally expressed as in equation (3) (the last term for [Mn(dota)]$^{2-}$ only):

$$[\mathrm{MnL}]_{\mathrm{tot}} = [\mathrm{MnL}] + [\mathrm{MnLZn}] + [\mathrm{MnHL}] + [\mathrm{MnH_2L}] \quad (3)$$

The pseudo-first-order rate constants, k_{obs}, is defined by equations (4) (Mn**L**^{2}, Mn**L**^{3} and [Mn(nota)]$^{-}$) and equation (5) ([Mn(dota)]$^{2-}$), respectively:

$$k_{\mathrm{obs}} = \frac{k_0 + k_1[\mathrm{H}^{+}] + k_2[\mathrm{H}^{+}]^2 + k_3[\mathrm{Zn}^{2+}] + k_4[\mathrm{H}^{+}][\mathrm{Zn}^{2+}]}{1 + K_{\mathrm{MnHL}}[\mathrm{H}^{+}] + K_{\mathrm{MnLZn}}[\mathrm{Zn}^{2+}]} \quad (4)$$

$$k_{obs} = \frac{k_0 + k_1[H^+] + k_2[H^+]^2 + k_3[Zn^{2+}] + k_4[H^+][Zn^{2+}] + k_5[H^+]^3 + k_6[H^+]^2[Zn^{2+}]}{1 + K_{MnHL}[H^+] + K_{MnH2L}[H^+]^2 + K_{MnLZn}[Zn^{2+}]} \quad (5)$$

where $k_0 = k_{MnL}$, $k_1 = k_{MnHL} \cdot K_{MnHL}$, $k_2 = k_{MnH2L} \cdot K_{MnHL} \cdot K_{MnH2L}$ (for $[Mn(dota)]^{2-}$) or $k_2 = K_{MnHL} \cdot {}^{H}k_{MnHL}$ (for the others), $k_3 = k_{MnLZn} \cdot K_{MnLZn}$, $k_4 = {}^{Zn}k_{MnHL} \cdot K_{MnHL}$, $k_5 = {}^{H}k_{MnH2L} \cdot K_{MnHL} \cdot K_{MnH2L}$ and $k_6 = {}^{Zn}k_{MnH2L} \cdot K_{MnHL} \cdot K_{MnH2L}$.

The observed rate constants for the complexes studied were fitted to equations (4) and (5) and the calculated parameters are listed in Table 3. During the fitting procedure, the values of the stability constants of the monoprotonated complexes $MnH\mathbf{L}^2$, $MnH\mathbf{L}^3$, [Mn(Hnota)] and $[Mn(Hdota)]^-$ or diprotonated $[Mn(H_2dota)]$ were fixed to the values obtained by potentiometry. Recently, the X-ray structure of this diprotonated $[Mn(H_2dota)]$ complex with two protonated and uncoordinated acetate arms has been published.[28]

Table 3 Kinetic parameters for the dissociation of $Mn\mathbf{L}^2$, $Mn\mathbf{L}^3$, $[Mn(nota)]^-$ and $[Mn(dota)]^{2-}$ in comparison to those for analogous Gd^{3+} complexes.

	Mn^{2+}				Gd^{3+}		
Parameters	$\mathbf{L}^2$	$H\mathbf{L}^3$	NOTA	DOTA	NOTA[a]	DOTA[b]	DTPA[c]
k_0 / s^{-1}	–[d]	–[d]	$(2.6 \pm 0.5) \times 10^{-6}$	$(1.8 \pm 0.6) \times 10^{-7}$	8.3×10^{-6}	5.0×10^{-10}	–
k_1 / M^{-1} s^{-1}	423 ± 31	2020 ± 40	$(7.8 \pm 0.1) \times 10^{-1}$	$(4.0 \pm 0.6) \times 10^{-2}$	2.3×10^{-2}	2.0×10^{-5}	0.58
k_2 / M^{-2} s^{-1}	$(1.0 \pm 0.3) \times 10^7$	$(8.0 \pm 0.3) \times 10^7$	–[d]	$(1.6 \pm 0.1) \times 10^3$	–	–	9.7×10^4
k_3/ / M^{-1} s^{-1}	–[d]	–[d]	$(1.1 \pm 0.5) \times 10^{-5}$	$(1.5 \pm 0.3) \times 10^{-5}$	–	–	5.6×10^{-2}
k_4 / M^{-2} s^{-1}	$(1.7 \pm 0.1) \times 10^4$	–[d]	–[d]	–[d]	–	–	–
K_{MnLZn}	–[d]	–[d]	3.6 ± 0.7	68 ± 6	–	–	K_{GdLZn}=7
$\log K_{MHL}$[e]	4.27	4.95	2.87	4.26	–	–	2
$\log K_{MH2L}$[e]	–	–	–	2.99	–	–	–
$t_{½}$ (pH 6.0, $c(Zn^{2+})$= 10^{-3} M)	26 min	6 min	58 h	868 h	23 h	3.7×10^5 h	3.4 h
$t_{½}$ (pH 6.0, $c(Zn^{2+})$= 10^{-5} M)	27 min	6 min	58 h	869 h	23 h	3.7×10^5 h	156 h
$t_{½}$ (pH 7.4, $c(Zn^{2+})$= 10^{-3} M)	11.0 h	144 min	74 h	1024 h	23 h	3.8×10^5 h	3.5 h
$t_{½}$ (pH 7.4, $c(Zn^{2+})$= 10^{-5} M)	11.4 h	144 min	74 h	1037 h	23 h	3.8×10^5 h	330 h

[a] ref.72. [b] 37 °C, transmetallation with Eu^{3+}, ref. 73. [c] ref. 74. [d] fixed to zero during the fitting procedure. [e] fixed to the value obtained from potentiometry.

All possible dissociation pathways (Scheme 4) have been considered but the fit of k_{obs} values revealed clearly that several terms have no influence and can be neglected. These comprise the terms with k_0 and k_3 for Mn**L**^{2}, terms with k_0, k_3 and k_4 for Mn**L**^{3}, k_2 and k_4 for $[Mn(nota)]^-$ and k_4, k_5 and k_6 for $[Mn(dota)]^{2-}$. If these dissociation pathways were taken into account during the fitting procedure, very small or negative values of the corresponding rate constants with very large errors have been obtained.

For Mn**L**^{3}, only k_1 and k_2, corresponding to the spontaneous and proton-assisted dissociation of monoprotonated complex, were calculated during the fitting. The dissociation of Mn**L**^{2} proceeds also *via* pathways including only protonated species: the spontaneous and proton-assisted dissociation of the monoprotonated complex (k_1 and k_2) and the zinc-assisted dissociation of the monoprotonated complex (k_4). For $[Mn(nota)]^-$, it was possible to calculate the rate constants k_0 and k_1 corresponding to the spontaneous dissociation of the non-protonated and the monoprotonated complexes as well as a low stability constant for the dinuclear complex, K_{MnLZn} = 3.9, which dissociates with a small rate constant k_3 (Table 3). In the case of $[Mn(dota)]^{2-}$, the fit led to reliable values for k_0, k_1, k_2 (k_2 represents the spontaneous dissociation of the diprotonated complex) as well as to the stability constant of the dinuclear complex, K_{MnLZn}, and the corresponding dissociation rate constant, k_3 (Table 3).

For Mn**L**^{3} , k_0 had to be fixed to zero in the fit, otherwise negative values were obtained. Thus, the spontaneous dissociation of the non-protonated complex does not contribute to the overall dissociation. It proceeds exclusively *via* pathways involving the monoprotonated complex represented by the calculated constants k_1 and k_2. Although zinc-assisted dissociation pathways (represented by k_3 and k_4) have been also involved, the fit revealed their negligible influence on the overall dissociation. For a better comparison of the kinetic inertness of the chelates, the dissociation half-times for different Zn^{2+} concentrations at pH 6 and 7.4 have been calculated. At physiological pH and blood Zn^{2+} concentration (pH 7.4 and $c(Zn^{2+}) = 10^{-5}$ M), the dissociation proceeds exclusively *via* the spontaneous dissociation of the protonated complex (represented by k_1).

Similar results have been obtained for the dissociation kinetics of Mn**L**^{2} except the positive influence of increasing Zn^{2+} concentration. The value of k_0 was close to zero showing that the spontaneous dissociation has no influence on the overall dissociation. The pathways related to k_1, k_2, k_4 involving the monoprotonated species were found to play a more important role in the overall complex dissociation. The direct attack of Zn^{2+} on the complex has low probability due to the positive charge of the complex, to the lack of available donor atoms

for Zn^{2+} binding and to steric hindrance (the dinuclear complex would require the ring twisting). When considering this pathway in the fit, we obtained a very small stability constant for the dinuclear complex and unreliable rate constants for its dissociations. However, the overall dissociation becomes accelerated with increasing Zn^{2+} concentration which indicates a positive effect of Zn^{2+}. This observation can be explained by the significant contribution of the zinc-assisted dissociation of the monoprotonated complex (k_4). Despite the very high positive charge of the complex, a transition state including a dinuclear species could be reasonable, if we take into account that the monoprotonated Mn^{2+} complex possesses one uncoordinated protonated nitrogen atom and an unstable, four-coordinated Mn^{2+} ion. Similarly to Mn**L**^{3}, the dissociation of Mn**L**^{2} at simulated physiological conditions proceeds *via* the spontaneous dissociation of the protonated complex (represented by k_1) as well.

The observed rate constants for $[Mn(nota)]^{-}$ and $[Mn(dota)]^{2-}$ strongly increase with increasing acid concentration for all exchanging metal ion concentrations and the results for $[Mn(nota)]^{-}$ correspond more to a close-to-linear dependency of k_{obs} on the proton concentration. The rate constant k_1 was calculated for both complexes while k_2 only for $[Mn(dota)]^{2-}$. This difference is probably caused by a formation of the diprotonated Mn^{2+} complex of DOTA under experimental pH. In contrast to Mn**L**^{2} and Mn**L**^{3}, the spontaneous dissociation for $[Mn(nota)]^{-}$ and $[Mn(dota)]^{2-}$ is not negligible. The calculated dissociation half times show negligible dependency on Zn^{2+} concentration and less than 1 % contribution of the proton-assisted pathway (represented by k_1). According to this the spontaneous dissociation of non-protonated complex was found to be the most important dissociation pathway under simulated physiological conditions for both complexes. The ~15-fold difference in the $t_{1/2}$ values is related to the different k_0 constants.

Interestingly, the suppression of the dissociation rate with increasing Zn^{2+} excess has been observed for both these complexes. This trend is related to the formation of dinuclear Mn^{2+}–L–Zn^{2+} complexes. They compete with the protonated MnH_iL species and because they dissociate more slowly, the overall dissociation rate is decreased. This suppression becomes more evident at lower pH when the abundance of protonated complexes is higher than that of the dinuclear complex. Similar modulation of the dissociation rate has been previously described for the transmetallation of Gd^{3+} complexes with Eu^{3+}.[74,75] The higher value of the dinuclear complex stability constants for $[Mn(dota)]^{2-}$ is in good agreement with the more significant suppression for $[Mn(dota)]^{2-}$ than for $[Mn(nota)]^{-}$. In $[Mn(dota)]^{2-}$, the approach of Zn^{2+} can be facilitated by the higher negative charge and the increased flexibility of the non-coordinating acetate pendant arms. According to the results of the fitting of the k_{obs} data,

the negligible role of zinc-assisted dissociation of the mono- and diprotonated complexes $[Mn(Hdota)]^-$ and $[Mn(H_2dota)]^0$ (represented by k_5 and k_6) is probably caused by a lower tendency to form a dinuclear complex with the less negatively charged protonated complexes.

The overall dissociation rate is the highest for Mn**L**^{3} among the complexes studied, which can be related to the highest rate of spontaneous dissociation of the monoprotonated complex (k_1). Its value is 5-times higher than for Mn**L**^{2} and 3–5 orders of magnitude higher than for $[Mn(nota)]^-$ and $[Mn(dota)]^{2-}$. The difference in k_1 is mainly responsible for the much faster overall dissociation of Mn**L**^{3} and Mn**L**^{2} in comparison to the NOTA and DOTA complexes (Table 3). Indeed, the proton assisted dissociation of the monoprotonated complex of Mn**L**^{3} and Mn**L**^{2}, represented by k_2, contributes at most 13 % (Mn**L**^{2}) or 23 % (Mn**L**^{3}) to the overall dissociation at the highest proton concentrations, so in overall it has little influence. The k_2 values for Mn**L**^{3} and for Mn**L**^{2} are comparable, while being several orders of magnitude higher than that obtained for $[Mn(dota)]^{2-}$. Zn^{2+} excess has no effect on the overall dissociation of Mn**L**^{3}, it accelerates the dissociation of Mn**L**^{2} and suppresses that of Mn^{2+} complexes of NOTA and DOTA. The most important structural factors that are responsible for the considerably faster dissociation of Mn**L**^{2} and Mn**L**^{3} with respect to $[Mn(nota)]^-$ or $[Mn(dota)]^{2-}$are (i) the presence of water molecule(s) in the coordination sphere, (ii) the lower rigidity and (iii) the less packed (more "open") structure of the complexes.

The considerably faster dissociation of $[Mn(nota)]^-$ with respect to $[Mn(dota)]^{2-}$ is accounted for by the one order of magnitude higher values of k_0 and k_1 for $[Mn(nota)]^-$. Especially at lower pH the spontaneous dissociation of diprotonated complex $[Mn(H_2dota)]$ (k_2) significantly accelerates the overall dissociation. The mechanism of the spontaneous and the proton-assisted dissociation of $[Mn(nota)]^-$ and $[Mn(dota)]^{2-}$ likely involves intermediates with one uncoordinated nitrogen macrocyclic atom, which is nonprotonated for the spontaneous and protonated (after proton transfer from the carboxylic acid group in the pendant arm) for the proton-assisted pathway. In overall, the intermediates and reaction steps are considered to be the same as those found for the dissociation of Gd^{3+} analogue complexes.[72,73]

When comparing Mn^{2+} and Gd^{3+} analogues, it is interesting to note that the k_0 and k_1 values are similar for [Gd(nota)] and $[Mn(nota)]^-$, and $[Mn(nota)]^-$ is even more inert under the simulated physiological conditions (Table 3). This can likely be accounted for the smaller ionic radius of Mn^{2+} which fits better to the relatively small cavity of the triazacyclononane-based ligand contrary to the larger Gd^{3+} ion having an uncompleted coordination sphere. The

several orders of magnitude higher dissociation half-time for $[Gd(dota)]^-$ than for $[Mn(dota)]^{2-}$ shows the extraordinary kinetic inertness of this Gd^{3+} complex. According to the calculated half-times, Mn**L**^{2} and Mn**L**^{3} dissociate much faster than these Gd^{3+} complexes. However, the dissociation half-time for Mn**L**^{2} under simulated physiological conditions is 11.4 h (pH 7.4, $c(Zn^{2+})=10^{-5}$ M) which indicates that the complex should stay intact during the course of an MRI experiment. Indeed, the typical elimination times for low-molecular-weight Gd^{3+} chelates are few hours for humans and few minutes for animals. For the dissociation of all Mn^{2+} complexes under simulated physiological conditions, the zinc-assisted pathways have no significance in comparison to $[Gd(dtpa)]^{3-}$ which can be attributed to the structure of the macrocyclic ligand which is less accessible for dinuclear complex formation than in the case of the open-chain ligand.

In conclusion, $[Mn(nota)]^-$ and $[Mn(dota)]^{2-}$ have dissociation half-times comparable to those for [Gd(nota)] and $[Gd(dtpa)]^{3-}$ which evidenced for the first time that not all Mn^{2+} complexes are kinetically labile, as it was previously supposed on the basis of *in vivo* studies.[14] Nevertheless, the other Mn^{2+} complexes studied are kinetically labile, except Mn**L**^{2} and Mn**L**^{3}.

Electrochemistry and oxidation state manganese(III)

The relaxivity of a Mn^{2+} complex can be strongly reduced by the oxidation of Mn^{2+} to the lower spin Mn^{3+} (less paramagnetic). In Mn^{2+} chemistry, the tendency of Mn^{2+} complexes to oxidize is rather common. In order to investigate the stability of the complexes studied towards air oxidation and to ensure the lack of Mn^{3+} species, cyclic voltammetry measurements have been performed. The cyclic voltammograms of 1mM complex solutions in 0.05 M KCl (supporting electrolyte) at pH = 8 (adjusted by KOH) were measured. The oxidation and reduction peaks of Mn**L**^{1} (E_{ox} = 1.11 V and E_{red} = 0.94 V *vs.* NHE) and Mn**L**^{2} (E_{ox} = 1.24 and E_{red} = 1.01 *vs.* NHE) represent a quasi-reversible couple $Mn^{III}L/Mn^{II}L$. The high value of the formal potentials correspond to the data published previously for Mn**L**^{2} in anhydrous MeOH ($E_{1/2}$ ~0.8 V)[64] and for $[Mn(Me_2\text{-}15\text{-}pyN_5)]^{2+}$ in aqueous HEPES buffer (HEPES = 4-(2-hydroxyethyl)-1-piperazine ethanesulfonic acid).[76]

The voltammograms recorded for Mn**L**^{3} and Mn**L**^{4} exhibit oxidation peaks at potentials E_{ox} = 0.73 V for Mn**L**^{3} and E_{ox} = 0.68 V for Mn**L**^{4} (vs. NHE) pointing to irreversible processes (Fig. 12). The absence of reduction peaks in the voltammograms can be explained by a slow kinetics of the electron transfer caused by a modification of the active species – at

pH 8 mainly the Mn^{3+} monohydroxocomplex exists (confirmed by X-ray structure of [Mn(**L**^{4})(OH)]).

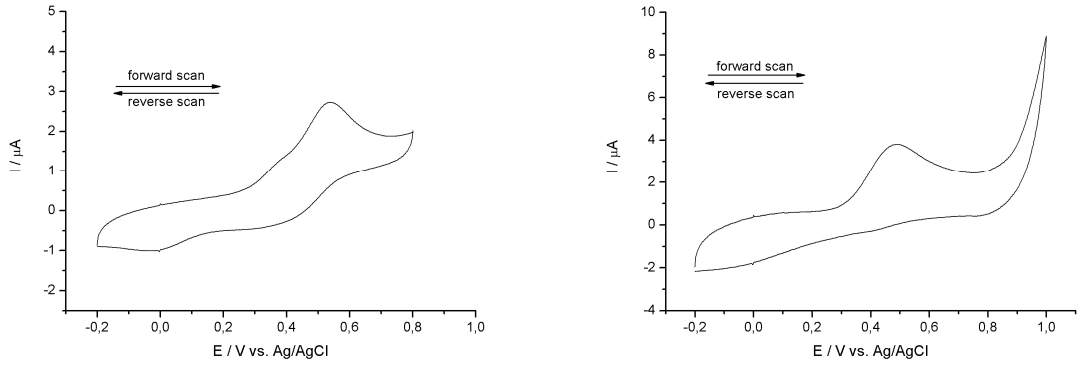

Figure 12 The cyclic voltammograms of the Mn^{2+} complexes of H**L**^{3}(a) and H_2**L**^{4}(b) (0.05 M KCl, pH = 8.0, 100 mV s^{-1})

The cyclic voltammograms of Mn**L**^{5}–Mn**L**^{8} were identical and showed only the catodic and anodic peaks at high positive potentials with large peak separation (E_{ox} ~ 1250 mV, E_{red} ~ 950 mV) which were attributed to non-complexed Mn^{2+}.

The stability of the Mn^{2+} complex toward air-oxidation is related to the difference between the formal redox potential of the complex and the potential of molecular oxygen (~0.8 V, differs with pH). The tendency or the rate of the oxidation depends on the experimental conditions and on the kinetics of the reaction. The formal redox potentials obtained for Mn**L**^{1} and Mn**L**^{2} are slightly higher than those for the air-stable $[Mn(nota)]^-$ (E = 0.74 V, ΔE = 94 mV) and $[Mn(edta)(H_2O)]^{2-}$ (E = 0.81 V) complexes.[77] These high formal redox potentials for Mn**L**^{1} and Mn**L**^{2} and the lack of any signal at potentials lower than ~0.8 V for Mn**L**^{5}–Mn**L**^{8} indicate good complex stability toward air-oxidation. The absence of any color change and the constant relaxivity over a long period of time supports this conclusion and confirms their redox stability under the experimental conditions used in the kinetic and NMR studies. On the other hand, Mn**L**^{3} and Mn**L**^{4} have been proven to undergo oxidation under air. Their redox potentials were below ~0.8 V and were lower than that for other air-stable complexes. Mn^{3+} complexes with ligands based on aminocarboxylates have not been much investigated and there are few examples of stable Mn^{3+} complexes like the NOTA propionate analogue NOTPr (E = 0.49 V, ΔE = 68 mV).[77] The higher oxidation peak potential of Mn**L**^{3} indicates the higher stability of the coordinated divalent manganese in comparison to Mn**L**^{4}. The phosphonate pendant arm in **L**$^{4(2-)}$ with an electron-donating effect causes a stronger ligand field than **L**$^{3(1-)}$ and therefore the tendency of oxidation to a Mn^{3+} complex is higher for Mn**L**^{4}. Other indication of the oxidation was a color change (colorless → red-orange)

of their solution upon exposure to air. In the time-dependent UV-VIS spectra, an absorption increase has been observed at ~440 nm (Fig. 13). These changes confirmed the faster oxidation of Mn**L**^{4} which agrees well with the lower value of the formal redox potential.

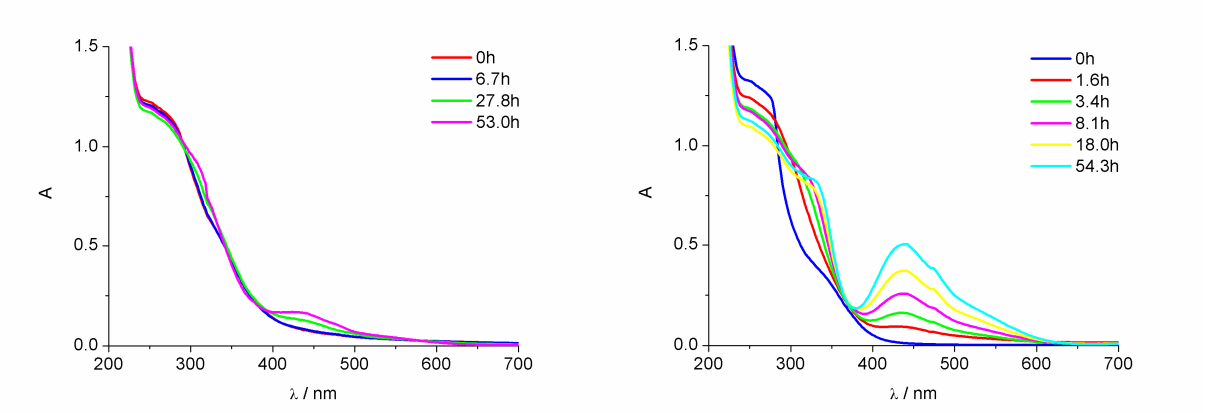

Fig. 13 UV-VIS spectra of Mn**L**^{3} (a) and Mn**L**^{4} (b) recorded in time after exposure to air.

Additionally, after exposure of the complex solution to air, the relaxivity dramatically dropped (Fig. 14) which is caused by the oxidation to Mn^{3+} and substitution of the water molecule by a hydroxo anion, in slow exchange with the bulk.

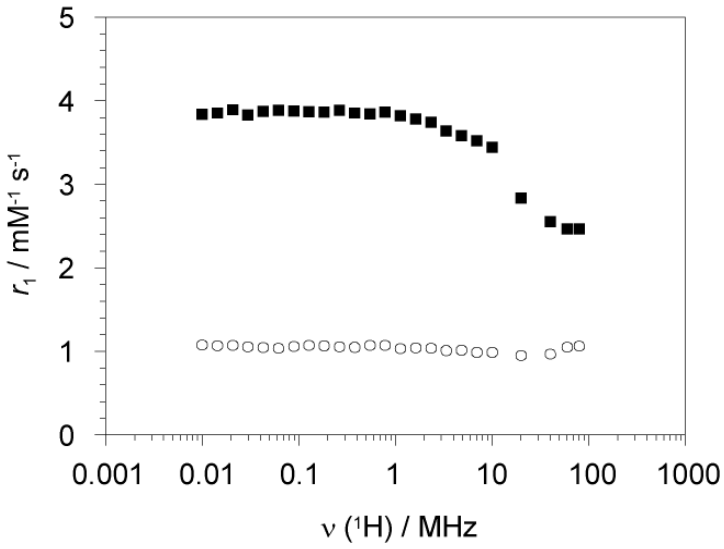

Fig. 14 ^{1}H NMRD profiles of Mn**L**^{4} (0.1 M TRIS, pH = 8, 25 °C) measured before (■) and after (○) exposure to air.

^{1}H NMRD and ^{17}O NMR measurements

Proton relaxivities measured as a function of the magnetic field represent the so-called Nuclear Magnetic Relaxation Dispersion profile which is a powerful and widely used tool for characterization of MRI CAs. The shape of the ^{1}H NMRD profile depends on the microscopic parameters governing the relaxivity and can help to distinguish between various relaxation mechanisms. In addition, variable-temperature ^{17}O NMR is often performed to independently access some of the parameters determining relaxivity. The temperature dependence of the ^{17}O transverse relaxation rates gives a direct access to the water exchange rate, k_{ex} (or water residence time $t_M = 1/k_{ex}$), whereas the dependence of the longitudinal relaxation rates informs about the rotational motion, described by the rotational correlation time, t_M. ^{17}O chemical shifts (w) are related to the hydration number of the complex.

The ^{1}H NMRD profiles were recorded for 5mM solutions of Mn**L**^{1}–Mn**L**^{8} at 25 and 37 °C (also at 50 and 65 °C for Mn**L**^{1} and Mn**L**^{2}, Fig. 15). Except for Mn**L**^{7} and Mn**L**^{8}, the shape of the profiles is typical of low-molecular-weight chelates with one dispersion between 1–10 MHz that originates from the dipolar contribution. The profiles of Mn**L**^{7} and Mn**L**^{8} show a second dispersion at low field ~0.1 MHz arising from a contact interaction. Similar curves have been previously observed only for free $[Mn(H_2O)_6]^{2+}$ (ref.[19]) and $[Mn_2(enota)(H_2O)_2]$.[26] Since this second dispersion decreased with ligand excess, it was attributed to the presence of free Mn^{2+} which is in accordance with the low thermodynamic stability and incomplete formation of these complexes even with 2-fold ligand excess. For this reason, Mn**L**^{7} and Mn**L**^{8} have been excluded from further NMR measurements where the presence of Mn^{2+} would mislead the interpretation of the experimental results.

The variable-temperature transverse ^{17}O relaxation times and chemical shifts were measured on aqueous solution of Mn**L**^{1}–Mn**L**^{6} at pH 8 which ensures full complex formation. The lack of free Mn^{2+} was ensured by using a ligand excess. The longitudinal relaxation times were also measured but they were not included in the treatment of the ^{17}O NMR results because the difference between the complex solution and the diamagnetic reference was too small (3–5 %), giving large errors in the reduced relaxation rates.

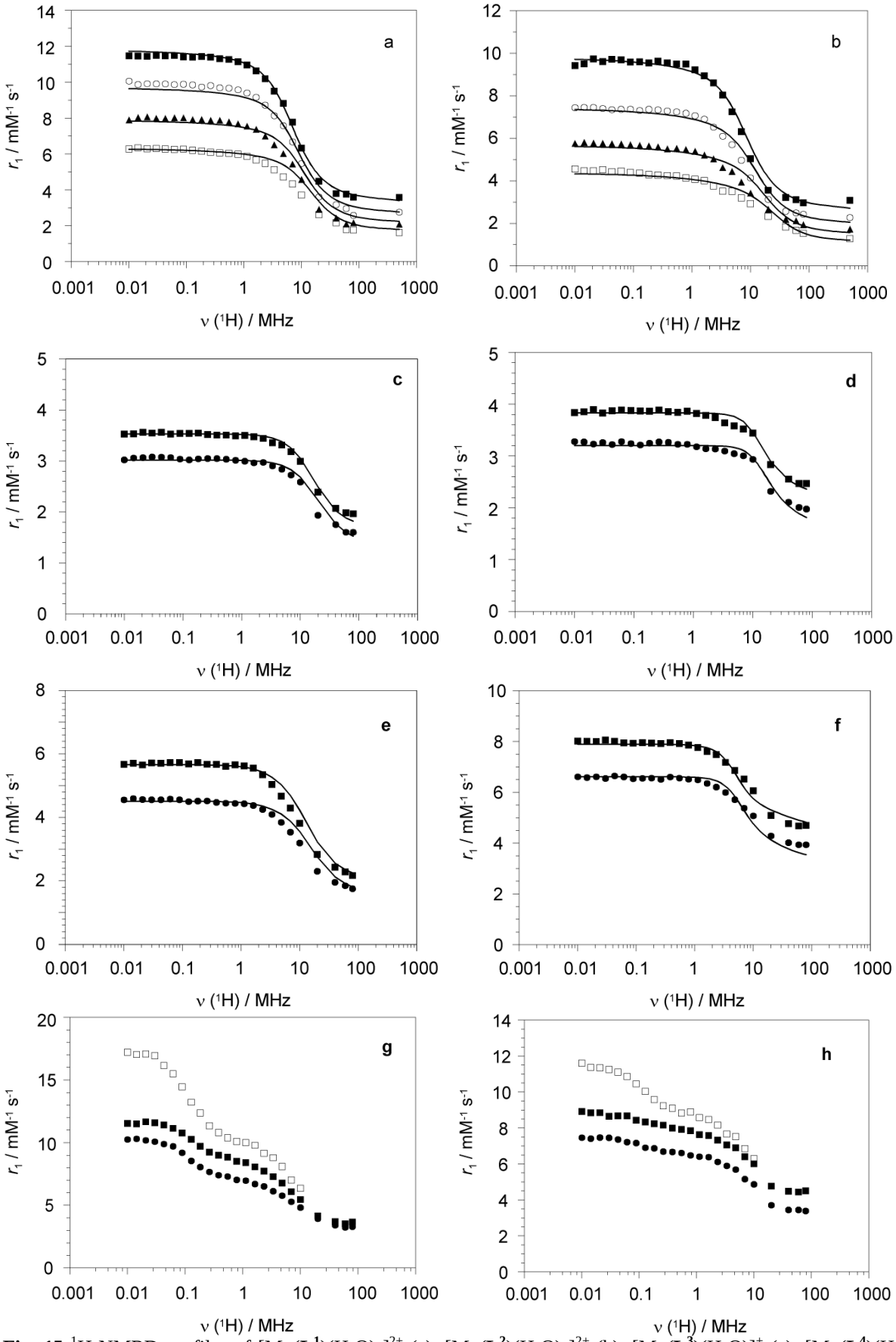

Fig. 15 ^{1}H NMRD profiles of $[Mn(\mathbf{L}^1)(H_2O)_2]^{2+}$ (a), $[Mn(\mathbf{L}^2)(H_2O)_2]^{2+}$ (b), $[Mn(\mathbf{L}^3)(H_2O)]^{+}$ (c), $[Mn(\mathbf{L}^4)(H_2O)]$ (d), $[Mn(\mathbf{L}^5)(H_2O)_x]$ (e), $[Mn(\mathbf{L}^6)(H_2O)]^{2-}$ (f), Mn–$\mathbf{L}^7$ (g) and Mn–$\mathbf{L}^8$ (h) systems measured at 25 (■), 37 °C (●,○) (c_{Mn2+} = 5mM, 0.1M TRIS, pH 8.0; for (a,b) 50 (▲) or 65 °C (□); for (g,h) 100% (■,●) or 25% (□) ligand excess).

Based on the crystal structures obtained, the Mn^{2+} complexes of $\mathbf{L^1}$ and $\mathbf{L^2}$ were assumed to have two inner-sphere water molecules, while the others were expected to be monohydrated. The measured ^{17}O chemical shifts were in full accordance with this hypothesis, except for Mn$\mathbf{L^5}$. The chemical shift data are proportional to the number of coordinated water molecules in the fast water exchange regime which can be confirmed by a successful data fitting with a scalar coupling constant having almost constant value for all Mn^{2+} complexes ($A_O/\mathbf{h}$ = 33–39 × 10^6 rad s^{-1}). A different value of the scalar coupling constant indicates difference in the hydration state like a hydration equilibrium observed for Mn$\mathbf{L^5}$. Equilibrium between mono- and bis-hydrated species (overall coordination numbers of 6 or 7 for Mn^{2+}) had to be considered otherwise the fitted curve did not reproduce the experimental data points measured for Mn$\mathbf{L^5}$. Therefore we assumed equation $\ln K = \Delta S^0/R - \Delta H^0/RT$ to define the equilibrium constant K and the chemical shifts have been fitted with a scalar coupling constant fixed to $A_O/\mathbf{h}$ = 33.3 × 10^6 rad s^{-1}. This allowed the

Table 4 Relaxivity and best fit parameters obtained from the simultaneous analysis of ^{17}O NMR and ^1H NMRD data for the investigated complexes Mn$\mathbf{L^1}$–Mn$\mathbf{L^6}$ compared to those for Mn^{2+} complex with ENOTA and Mn^{2+} aquaion.

Parameter	$[Mn(\mathbf{L^1})(H_2O)_2]^{2+}$	$[Mn(\mathbf{L^2})(H_2O)_2]^{2+}$	$[Mn(\mathbf{L^3})(H_2O)]^{+}$	$[Mn(\mathbf{L^4})(H_2O)]$
r_1 at 25/37 °C (20 MHz) / mM^{-1} s^{-1}	4.48 / 3.61	3.56 / 3.13	2.39 /1.94	2.84 / 2.32
k_{ex}^{298} / 10^7 s^{-1}	0.38 ± 0.2	6.9 ± 0.7	303 ± 19	177 ± 9
$\Delta H^{\ddagger}$ / kJ mol^{-1}	35.3 ± 2	37.7 ± 4	13.0 ± 1.6	14.0 ± 1.2
E_{rH} / kJ mol^{-1}	16.1 ± 0.5	23.1 ± 0.5	16.0 ± 2.6	20.3 ± 2.1
τ_{rH}^{298} / ps	40.3 ± 5	28.3 ± 5	23.0 ± 1.8	38.6 ± 1.9
τ_v^{298} / ps	3.3 ± 0.5	3.9 ± 0.2	8.7 ± 0.8	14.3 ± 0.6
Δ^2 / 10^{18} s^{-2}	6.6 ± 0.5	4.6 ± 0.1	40.0 ± 5	302 ± 11
$A_O/\mathbf{h}$ / 10^6 rad s^{-1}	38.6[a]	38.6 ± 4	36.6 ± 1.3	39.9 ± 1.7

	$[Mn(\mathbf{L^5})(H_2O)_x]$	$[Mn(\mathbf{L^6})(H_2O)]^{2-}$	$[Mn_2(ENOTA)(H_2O)_2]$[b]	$[Mn(H_2O)_6]^{2+}$ [c]
r_1 at 25/37 °C (20 MHz) / mM^{-1} s^{-1}	2.83 / 2.30	5.08 / 4.29	3.39 / 2.71	7.4[d]/6.76[e]
k_{ex}^{298} / 10^7 s^{-1}	119 ± 22	1.20 ± 0.1	5.5	2.1
$\Delta H^{\ddagger}$ / kJ mol^{-1}	11.7 ± 0.8	38.8 ± 1.1	20.5	32.9
E_{rH} / kJ mol^{-1}	12 ± 1	23 ± 2	18	–
τ_{rH}^{298} / ps	22 ± 1	103 ± 2	26	30[f]
τ_v^{298} / ps	12.4 ± 0.6	33.7 ± 0.8	7.7	3.3
Δ^2 / 10^{18} s^{-2}	79 ± 5	53 ± 4	4.7	5.6
$A_O/\mathbf{h}$ / 10^6 rad s^{-1}	33.3[a]	33.3[a]	32.7	33.3

[a] fixed during the fitting procedure. [b] ref. 26. [c] ref. 78. [d] ref. 19. [e] ref. 28. [f] T = 308 K, ref. 79.

calculation of an average hydration number, q_{ave} (q_{ave} = {c([Mn($\mathbf{L}^5$)(H_2O)])×1 + c([Mn($\mathbf{L}^5$)(H_2O)$_2$])×2}/c_{MnL5}) as a function of the temperature. Based on this analysis, the average hydration number was found to vary between 1.1 and 1.7 in the temperature range of the ^{17}O NMR measurements. For more detailed justification see Appendix 3.

For all complexes, the reduced transverse ^{17}O relaxation rates and ^{17}O chemical shifts were fitted simultaneously with the ^{1}H NMRD data according to the Solomon-Bloembergen-Morgan theory of paramagnetic relaxation by assuming two inner-sphere water molecules for Mn$\mathbf{L}^1$ and Mn$\mathbf{L}^2$, one water molecule for Mn$\mathbf{L}^3$, Mn$\mathbf{L}^4$ and Mn$\mathbf{L}^6$ or by using the ΔH^o and ΔS^o values to calculate the average hydration number at each temperature for Mn$\mathbf{L}^5$. The best fit parameters obtained from the analysis are listed and compared with those for $[Mn(H_2O)_6]^{2+}$ and other relevant Mn^{2+} chelates in Table 4 (equations used in the data analysis are given in the Supporting information in Appendixes).

The water exchange rates calculated for the complexes Mn$\mathbf{L}^1$–Mn$\mathbf{L}^6$ are in accordance with the shape of the temperature dependent ^{17}O transverse relaxation rates (fast or slow water exhange regime). Very slow water exchange rate was found for Mn$\mathbf{L}^1$ ($k_{ex}^{298} = 0.38 \times 10^7\ s^{-1}$), the slowest ever reported on a Mn^{2+} complex. The water exchange on Mn$\mathbf{L}^2$ and Mn$\mathbf{L}^6$ is in slow to intermediate exchange regime and the values are in the typical range of previously studied complexes ($k_{ex}^{298} \sim 10^7\ s^{-1}$). On the other hand, an extremely fast water exchange was observed on Mn$\mathbf{L}^3$–Mn$\mathbf{L}^5$. The values of k_{ex}^{298} are about two orders of magnitude higher and $k_{ex}^{298} = 303 \times 10^7\ s^{-1}$ for Mn$\mathbf{L}^3$ is the highest exchange rate ever reported. $[Mn(nta)(H_2O)_2]^-$ is the only example of a complex with similarly fast water exchange (Table 5). The differences in the water exchange rates are rather difficult to explain. In general, the presence of a phosphonate functional group in the ligand pendant arm significantly decreases the exchange rate of the Mn^{2+} complex (Mn$\mathbf{L}^4$ and Mn$\mathbf{L}^6$ in comparison to Mn$\mathbf{L}^3$ and Mn$\mathbf{L}^5$), which can be explained by the hydrophilic nature of the phosphonate functional group with a tendency to form hydrogen bonds. Slower water exchange rate was also observed for the complexes with ligands containing oxygen instead of nitrogen donor atom in the macrocyclic scaffold.

To assess the mechanism of the water exchange, variable-pressure ^{17}O transverse relaxation rate measurements have been performed. This technique allows for determining the activation volume of the water exchange, $\Delta V^{\ddagger}$, which is the most significant parameter enabling to distinguish between various water exchange mechanism. The activation volumes together with other relevant water exchange parameters are summarized in Table 5. The mechanism of the water exchange is closely related to the coordination number of Mn^{2+}. It

has been previously observed that the water exchange on Mn^{2+} complexes with CN = 7 proceeds *via* a dissociative whereas with CN = 6 *via* an associative mechanism. In accordance with this, the positive activation volume for Mn**L**^{2} (CN = 7) indicates a dissociatively activated mechanism whereas the negative values for Mn**L**^{3}, Mn**L**^{4} and Mn**L**^{6} (CN = 6) demonstrate the associative character of the water exchange. On the other hand, the activation volume is zero for Mn**L**^{1} with CN = 7 indicating a pure interchange mechanism. For Mn**L**^{5}, the evaluation of the data is complicated by the equilibrium between two species with different coordination numbers but finally the contribution of the complex with CN = 7 with a dissociative mechanism prevailed (some simplifications were done, however, in the analysis; the average hydration number was considered constant). The results obtained for Mn**L**^{1}–Mn**L**^{4} are further supported by the calculated values of the activation entropy which have the same sign as the activation volumes. In general, the activation volumes are small (far from the limiting values) and correspond rather to associative interchange (I_a) or dissociative interchange (I_d) mechanisms.

Table 5 Comparison of the parameters related to the water exchange for various Mn^{2+} complexes and aqua ion.

	CN	k_{ex}^{298} / 10^7 s^{-1}	$\Delta H^{\ddagger}$ / kJ mol^{-1}	$\Delta S^{\ddagger}$ / J mol^{-1} K^{-1}	$\Delta V^{\ddagger}$ / cm^3 mol^{-1}	ref.
$[Mn(\mathbf{L}^{1})(H_2O)_2]^{2+}$	7	0.38 ± 0.2	35.3 ± 2	–1.0 ± 6	– 0.1 ± 0.1	this work
$[Mn(\mathbf{L}^{2})(H_2O)_2]^{2+}$	7	6.9 ± 0.7	37.7 ± 4	+32 ± 12	+1.6 ± 0.1, +3.2	this work 65
$[Mn(\mathbf{L}^{3})(H_2O)]^{+}$	6	303 ± 19	13.0 ± 1.6	– 20 ± 3	–5.4 ± 0.3	this work
$[Mn(\mathbf{L}^{4})(H_2O)]$	6	177 ± 9	14.0 ± 1.6	– 21 ± 2	–4.9 ± 0.2	this work
$[Mn(\mathbf{L}^{5})(H_2O)_x]$	6/7	119 ± 22	11.7 ± 0.8	–32 ± 5	+5.1 ± 0.2	this work
$[Mn(\mathbf{L}^{6})(H_2O)]^{2-}$	6	1.20 ± 0.1	38.8 ± 1.1	+23 ± 3	– 4.4 ± 0.1	this work
$[Mn(H_2O)_6]^{2+}$	6	2.1	32.9	+5.7	–5.4	78
Mn_2(enota)$(H_2O)_2]$	6	5.5	20.5	–28	–10.7	26
$[Mn(nta)(H_2O)_2]^{-}$	6	150	32.1	+29	–	80
$[Mn(edta)(H_2O)]^{2-}$	7	41	36.6	+43	+3.4	81

The relaxivities of the reported Mn^{2+} complexes strongly depend on the hydration number. The monohydrated complexes Mn**L**^{3}–Mn**L**^{5} have about twice as low relaxivites as the bishydrated Mn**L**^{1} and Mn**L**^{2} and correspond to that found for other monohydrated complexes, *e.g.* $[Mn(edta)(H_2O)]^{2-}$.[19] Nevertheless, one monohydrated complex, Mn**L**^{6}, has similar relaxivity as bishydrated complexes. This discrepancy is attributed to a longer value calculated for the rotational correlation time (τ_{rH}^{298} = 103 ps, longer than typical values corresponding to low-molecular-weight chelates). This might reflect a probable second-sphere

relaxation effect induced by the phosphonate functional groups. Without any information about the parameters characterizing the second coordination sphere, the second-sphere contribution is difficult to quantify and therefore was rather neglected and the fit therefore led to an artificially high value of the rotational correlation time. On the other hand, intermolecular interactions between the Mn**L**^{6} species can not be excluded either, since phosphonate groups are known to tend to oligomerise and form aggregates. The relaxivities of Mn**L**^{1}, Mn**L**^{2} and Mn**L**^{6} are comparable with those for commercially available contrast agents based on Gd^{3+} chelates with one inner-sphere water molecule ($[Gd(dota)(H_2O)]^-$: r_1 = 4.2 mM^{-1} s^{-1}; $[Gd(dtpa)(H_2O)]^{2-}$: r_1 = 4.3 mM^{-1} s^{-1}).

Ternary complex formation with endogenous anions

Small endogenous anions like phosphate, carbonate, citrate or lactate are capable to irreversibly replace the inner-sphere water molecule(s) from metal complexes which can be strongly limitative for *in vivo* relaxivity of the chelates. These anions are usually coordinated in a bidentate manner and therefore this exchange is more probable for bishydrated complexes with two water molecules in adjacent position. Such replacement has been already observed *e.g.* for [Gd(do3a)].[82] Here, Mn^{2+} complexes of **L**^{1} and **L**^{2} have two inner-sphere water molecules, but in opposite apical positions. All other complexes have only one directly coordinated water molecule (Mn**L**^{5} has a fraction of a bishydrated form). This fact should decrease the probability of water displacement by bidentate anions.

The relaxivity of the Mn^{2+} complexes has been recorded in the presence of 1–100 equivalents of phosphate (mixture of HPO_4^{2-}/$H_2PO_4^-$), citrate (cit^{3-}/$Hcit^{2-}$) or carbonate (CO_3^{2-}/HCO_3^-) at pH 8 (Fig. 16). Carbonate has no effect on any of the complexes studied. For Mn**L**^{3} and Mn**L**^{4}, the presence of phosphate and citrate has no effect either (Fig. 16c). In the case of Mn**L**^{2}, the relaxivity decreased with increasing amounts of phosphate and citrate. The least-square fitting of the relaxivity plot versus [anion]/[complex] ratio allowed to estimate the binding constants, K = 20±5 M^{-1} for phosphate and K = 100±7 M^{-1} for citrate (Fig. 16b). These constants indicate a relatively weak binding of the anions (weaker than for complexes of DO3A derivatives). This can be related to non-adjacent position of the two inner-sphere water molecules which only allows for anion binding in a monodentate fashion.

For complexes Mn**L**^{1}, Mn**L**^{5} and Mn**L**^{6}, the relaxivity increased upon addition of phosphate or citrate (Fig. 16a). This relaxivity enhancement could be explained by the formation of some intermediates that finally lead to the decomposition of the complexes, since after one day the relaxivity drops down to the values of manganese(II) phosphate or

citrate and a precipitate is observed in the solution. These decomposition intermediates have non-identified structure, but their ^{1}H NMRD profiles show elevated relaxivities at all magnetic fields (1–80 MHz). A single dispersion between 1–10 MHz without a high-field relaxivity peak implies that there is no free Mn^{2+} present and there are no slowly tumbling aggregates, either. The decomposition of the complexes upon addition of the anions is a result of their low stability.

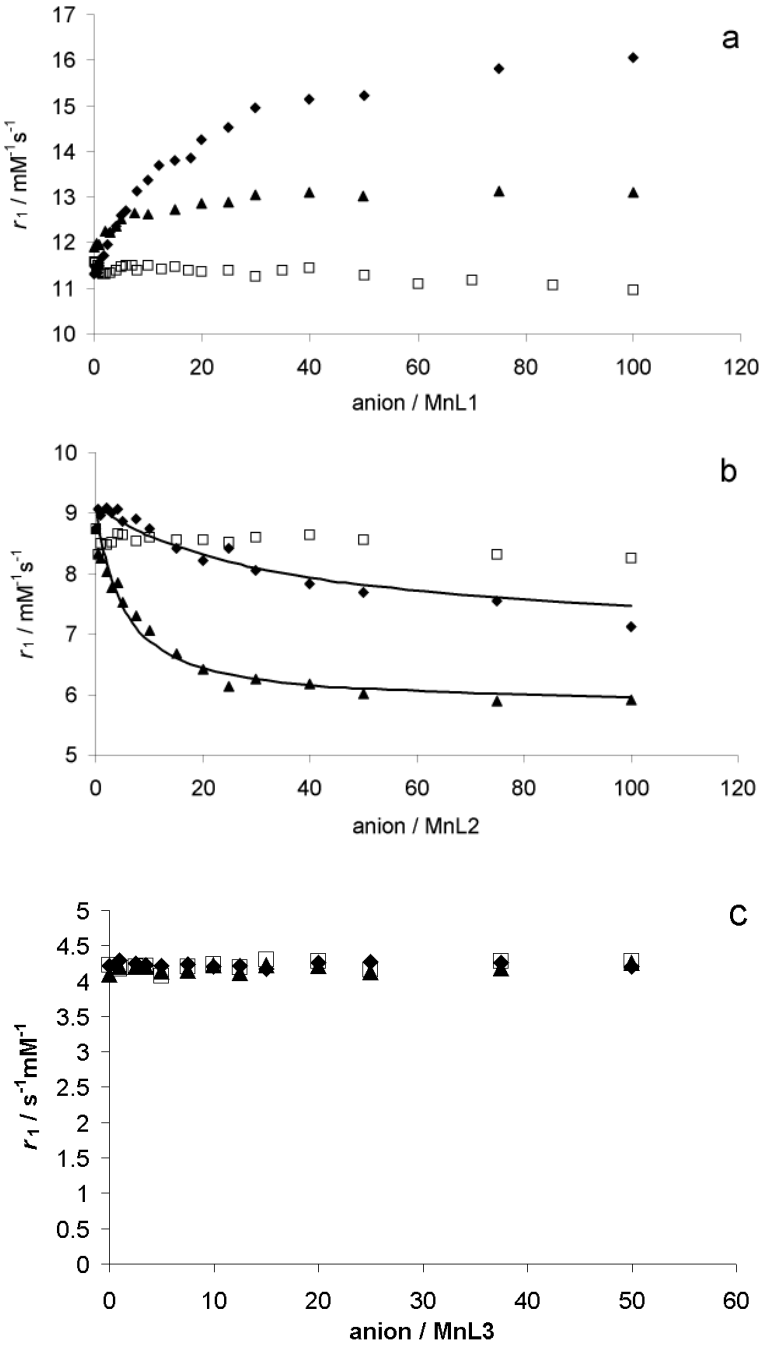

Fig. 16 ^{1}H relaxivities upon addition of phosphate (®), carbonate (□) and citrate (▲) to the solution of Mn**L**^{1} (a), Mn**L**^{2} (b) and Mn**L**^{4} (c) (0.1 M TRIS buffer, pH 8.0, 0.5 MHz, 25 °C).

Conclusions

In order to gain more insight into the relationships between ligand structure, stability and relaxation properties of Mn^{2+} complexes with respect to potential application as MRI contrast agents, three groups of complexes with structurally different ligands have been investigated. The dioxa-triaza or pentaza 15-membered pyridine based macrocycles (**L**^{1} or **L**^{2}) are without any pendant arms, the tetraaza 12-membered pyridine based ligands contain carboxylic (H**L**^{3}) or phosphonic acid (H_2**L**^{4}) functional group in one pendant arm, while the oxa-diaza 9-membered macrocycles are modified by two pendant arms bearing carboxylic acid (H_2**L**^{5}), phosphonic acid (H_4**L**^{6}), phosphinic acid (H_2**L**^{7}) or phenylphosphinic acid (H_2**L**^{8}) moieties. All ligands were prepared by standard synthetic procedures using well-known amino-protecting groups (tosyl, nosyl) and standard deprotecting agents. The coordination number of Mn^{2+} in the complexes has been confirmed by X-ray crystal structures. While Mn**L**^{1} and Mn**L**^{2} form pentagonal bipyramidal coordination spheres with CN = 7 for Mn^{2+}, all other complexes contain Mn^{2+} with CN = 6 adopting distorted octahedral coordination spheres. The pentadentate nature of the ligands allows the coordination of two inner-sphere water molecules in Mn**L**^{1} and Mn**L**^{2} and one water molecule in Mn**L**^{3}–Mn**L**^{8}.

The protonation constants of the ligands and the thermodynamic stability constants of their complexes with Mn^{2+} and other selected metal ions have been determined by equilibrium potentiometric titrations. The protonation sequence of H**L**^{3}, H_2**L**^{4} and H_2**L**^{7} was studied by ^{1}H and ^{31}P pH-NMR titration which revealed that the first two protonation steps (logK_{H1} and logK_{H2}) correspond to the protonation of the macrocyclic nitrogen atoms. The ligand basicity is reduced by the presence of the pyridine ring as well as by the atom substitution from nitrogen to oxygen (**L**^{2}→**L**^{1}, NO2A→H_2**L**^{5}). The functional group in the pendant arm also significantly influences the ligand basicity, which then increases in the following order: phosphinate< phenylphosphinate < acetate < phosphonate.

The stability constants (or the percentage of free non-complexed Mn^{2+}) show the highest thermodynamic stability for the complexes with **L**^{2}, H_2**L**^{4} and H**L**^{3} which are fully formed under physiological pH. On the other hand, Mn**L**^{7} and Mn**L**^{8} are not completely formed even for 2-fold ligand excess above pH 9. The ligands with all nitrogen donor atoms form more stable complexes, though Mn^{2+} is known as an oxophilic ion. The complex stability correlates with the increasing ligand basicity. Consequently, the stability increases with the ligand functional group in the same order as observed for the basicity: phosphinate< phenylphosphinate < acetate < phosphonate. Substitution of the nitrogen atom to oxygen

in the macrocyclic scaffold leads to a decrease in complex stability. On the other hand, the presence of the pyridine unit results in an enhancement of the complex stability which is also observed for the expansion of the ligand macrocyclic cavity.

Dissociation kinetic data were recorded only for Mn**L**^{2} and Mn**L**^{3} because the other complexes dissociate extremely rapidly under the experimental conditions. The dissociation of both Mn**L**^{2} and Mn**L**^{3} is very fast and proceeds mainly *via* pathways including protonated species. The dissociation of Mn**L**^{3} is independent while that of Mn**L**^{2} is accelerated by increasing Zn^{2+} concentration. Dissociation kinetics of Mn^{2+} complexes of NOTA and DOTA, well-known ligands in the context of MRI, were investigated as well. The results revealed considerable kinetic inertness of these Mn^{2+} complexes. Their dissociation rates were several orders of magnitude slower than those for Mn**L**^{2} and Mn**L**^{3} and comparable with [Gd(nota)] or $[Gd(dtpa)]^{2-}$. According to the dissociation half-times simulated for physiological conditions, the complex inertness increases in the order of Mn**L**^{3}<Mn**L**^{2} <$[Mn(nota)]^{-}$<$[Mn(dota)]^{2-}$ approximately in a ratio of 1: 5 : 35 : 500. In contrast to the results for Mn**L**^{2} and Mn**L**^{3}, the dissociation of $[Mn(nota)]^{-}$ and $[Mn(dota)]^{2-}$ is suppressed by increasing Zn^{2+} excess.

Mn**L**^{3} and Mn**L**^{4} are slowly oxidized to Mn^{3+} complexes by air-oxygen as evidenced by changes in the UV-VIS spectra, a relaxivity drop upon air-exposure and the low oxidation peak potentials obtained from the cyclic voltammetry. The complexes of the other ligands investigated were found to be inert toward air-oxidation.

The simultaneous fit of variable-temperature ^{17}O NMR and ^{1}H NMRD data provided information about the microscopic parameters governing the relaxivity. The rotational correlation times correspond to low-molecular-weight chelates except for Mn**L**^{6} with τ_r ~3 times longer. The water exchange rate varies in a wide range from the lowest for Mn**L**^{1} ($k_{ex}^{298} = 0.38 \times 10^{7}\ s^{-1}$) to the highest for Mn**L**^{3} ($k_{ex}^{298} = 3.03 \times 10^{9}\ s^{-1}$) ever reported for Mn^{2+} complexes. According to the activation volumes, $\Delta V^{\ddagger}$, obtained from variable-pressure ^{17}O NMR, an interchange or a dissociative interchange mechanism was found for the water exchange on Mn**L**^{1}, Mn**L**^{2} and Mn**L**^{5} (CN = 7 for Mn^{2+}) while an associative interchange mechanism was evidenced for Mn**L**^{3}, Mn**L**^{4} and Mn**L**^{6} (CN = 6). The correlation between the rate and mechanism of water exchange and the complex structure and charge appears complex and difficult to define. The relaxivities of Mn**L**^{3}, Mn**L**^{4} and Mn**L**^{5} correspond to the values previously observed for monohydrated complexes and are half of those for bishydrated Mn**L**^{1} and Mn**L**^{2}. The high relaxivity of Mn**L**^{6} is related to the long value of rotational correlation

time due to the presence of two phosphonate functional groups in the pendant arms (intermolecular interaction, possible second-sphere effect). Mn**L**^{1}, Mn**L**^{2} and Mn**L**^{6} have relaxivities comparable with those of monohydrated Gd^{3+} complexes with DOTA and DTPA.

The influence of small endogenous anions like phosphate, citrate of carbonate on the replacement of the water molecule in the complexes was monitored by relaxometry. The carbonate anion has no effect on any of the studied complexes. Phosphate and citrate replace one water molecule from the bishydrated Mn**L**^{2} (weak binding constants were calculated) or induce slow decomposition of Mn**L**^{1}, Mn**L**^{5} and Mn**L**^{6} accompanied by a short-term increase of relaxivity followed by a precipitation of manganese(II) phosphate or citrate after one day. No effect of either of the anions has been observed for Mn**L**^{3} and Mn**L**^{4}.

In conclusion, these results allow for establishing some trends of how the ligand structure, the rigidity of the ligand scaffold and its donor-acceptor properties influence the thermodynamic, kinetic and redox stability of the Mn^{2+} complex. The relaxation efficiency, expressed by the relaxivity, and in some cases even the hydration number of the complexes are hardly predictable. Many parameters which govern relaxivity of the Mn^{2+} complexes remain to be optimized in a similar way as it has been done for Gd^{3+} chelates. Nevertheless, the relaxivity of the bishydrated Mn^{2+} complexes and of Mn**L**^{6} are comparable to those of commercially available Gd^{3+} based contrast agents. On the other hand, further improvement remains to be achieved in the stability of Mn^{2+} complexes. When seeking for novel ligands suitable for Mn^{2+} complexation, polyaza macrocycles seem particularly well adapted. Attention has to be paid to find a balance between the thermodynamic stability, which is mainly influenced by the basicity of the ligand, and the redox properties of the complex, depending on the ligand charge and the size of the macrocyclic cavity.

Acknowledgement

First of all, let me acknowledge both my supervisors. I would like to thank to Prof. Ivan Lukeš for governing my doctoral work and for new chemistry topics and future visions. Thank to Dr. Eva Jakab Tóth for offering me an opportunity to spend a very nice time in her top-equipped laboratory in Orléans and for being a doctoral student of the University of Orléans as well. She helped me not only with one of the most difficult part of the work – NMR data fitting but she has been acting as a careful reviewer of all my papers. I thank her also for the help with my installation in France.

I would like to thank to all persons in the laboratory "19" in Prague, especially to Miroslav Pniok for the synthesis of 9-membered ligands and the measurement of MS, Jana Havlíčková for her help with the potentiometric titrations, Vojta Kubíček for the help to finish up the thesis and for MS measurements , Jan Kotek for solving the X-ray structures and reviewing my papers, Petr Hermann for being a rewiever of my papers and a source of new chemistry visions, Jan Plutnar for helping me with NMR.

I also thank to all people from the laboratory in Orléans, especially Thomas Chauvin for his help with ^{17}O NMR and ^{1}H NMRD, Célia Bonnet for her help with the ^{1}H NMRD and the kinetic experiments.

Dr. I. Císařová from Charles University in Prague is acknowledged for measuring of the X-ray data and Prof. J. Barek from Charles University in Prague for providing the electrochemistry equipment.

Prof. L. Helm from the Ecole Polytechique Fédérale de Lausanne in Switzerland is acknowledged for providing the high-pressure ^{17}O NMR equipment and helping me with the measurements.

Abbreviations

CA	Contrast Agent
CN	Coordination Number
DMF	*N,N'*-Dimethylformamide
EtOH	Ethanol
ESI	Electron Spray Ionization
THF	Tetrahydrofuran
HEPES	4-(2-hydroxyethyl)-1-piperazine ethanesulfonic acid
MALDI-TOF	Matrix-assisted Laser Desorption/Ionization – Time of Flight
MeCN	Acetonitrile
MEMRI	Manganese Enhanced Magnetic Resonance Imaging
MeOH	Methanol
MES	2-(4-morpholino)ethanesulfonic acid
MRI	Magnetic Resonance Imaging
NHE	Normal Hydrogen Electrode
NMR	Nuclear Magnetic Resonance
NMRD	Nuclear Magnetic Relaxation Dispersion
i-PrOH	2-Propanol (Isopropyl Alcohol)
RT	Room Temperature
SBM	Solomon–Bloembergen–Morgan
TFA	Trifluoroacetic acid
TLC	Thin Layer Chromatography
TMS	Tetramethylsilane
TRIS	Tris(hydroxomethyl)amino methane
UV-VIS	Ultraviolet-Visible

Structures of the studied ligands are shown in **Chart 2**. Structures of the other ligands discussed in the text are displayed in **Chart 1**.

References

1. *MRI Basic Principles and Applications*; M. A. Brown, R. C. Semelka, John Wiley & Sons: New Jersey, **2010**.
2. A. D. Sherry, P. Caravan and R. E. Lenkinski, *J. Magn. Reson. Imag.*, **2009**, *30*, 1240–1248.
3. M. Aschner, K. M. Erikson and D. C. Dorman, *Crit. Rev. Toxicol.*, **2005**, *35*, 1–32.
4. P. Caravan, J. J. Ellison, T. J. McMurry and R. B. Lauffer, *Chem. Rev.*, **1999**, *99*, 2293–2352.
5. P. Hermann, J. Kotek, V. Kubíček and I. Lukeš, *Dalton Trans.*, **2008**, 3027–3047.
6. E. Tóth and A. E. Merbach, *The Chemistry of Contrast Agents in Medical Magnetic Resonance Imaging*, John Wiley & Sons: Chichester, **2001**.
7. P. Caravan, *Chem. Soc. Rev.*, **2006**, *35*, 512–523.
8. P. C. Lauterbur, *Nature*, **1973**, *242*, 190–191.
9. D. W. Christianson, *Progr. Biophys. Mol. Biol.*, **1997**, *67*, 217–252.
10. F. C. Wedler and R. B. Denman, *Curr. Top. Cell Regul.*, **1984**, *24*, 153–169.
11. A. S. Mildvan and M. Cohn, *Biochemistry*, **1963**, *338*, 910–919.
12. J. Eisinger, F. Fawaz-Estrup and R. G. Shulman, *J. Chem. Phys.*, **1965**, *42*, 43–53.
13. M. G. Cersosimo and W. C. Koller, *NeuroToxicology*, **2006**, *27*, 340–346.
14. B. Gallez, C. Baudelet and M. Geurts, *Magn. Reson. Imag.*, **1998**, *16*, 1211–1215.
15. *NMR Biomed.*, **2004**, *17*, 527–634. The issue No. 8 is dedicated to the "Manganese Enhanced Magnetic Resonance Imaging (MEMRI)".
16. S. M. Rocklage, W. P. Cacheris, S. C. Quay, F. E. Hahn and K. N. Raymond, *Inorg. Chem.*, **1989**, *28*, 477–485.
17. U. Kettritz, J. F. Schlund, K. Wilbur, L. B. Eisenberg and R. C. Semelka, *Magn. Reson. Imag.*, **1996**, *14*, 1185–1190.
18. T. Murakami, R. L. Baron, M. S. Peterson, J. H., III. Oliver, P. L. Davis, B. S. Confer and M. P. Federle, *Radiology*, **1996**, *200*, 69–77.
19. S. H. Koenig, C. Baglin, R. D., III. Brown and C. F. Brewer, *Magn. Reson. Med.*, **1984**, *1*, 496–501.
20. J. Maigut, R. Meier, A. Zahl and R. van Eldik, *Inorg. Chem.*, **2008**, *47*, 5702–5719.
21. S. Aime, P. L. Anelli, M. Botta, M. Brocchetta, S. Canton, F. Fedeli, E. Gianolio and E. Terreno, *J. Biol. Inorg. Chem.*, **2002**, *7*, 58–67.
22. J. S. Troughton, M. T. Greenfield, J. M. Greenwood, S. Dumas, A. J. Wiethoff, J. Wang, M. Spiller, T. J. McMurry and P. Caravan, *Inorg. Chem.*, **2004**, *43*, 6313–6323.
23. A. Bertin, J. Steibel, A. I. Michou-Gallani, J. L. Gallani and D. Felder-Flesch, *Bioconjugate Chem.*, **2009**, *20*, 760–767.
24. (a) H. A. Tang, Y. Sheng and R. D. Yang, *Inorg. Chem. Commun.*, **2003**, *6*, 1213–1216; (b) D. W. Zhang, Z. Y. Yang, S. P. Zhang and R. D. Yang, *Trans. Metal Chem.*, **2006**, *31*, 333–336.
25. C. F. G. C. Geraldes, A. D. Sherry, R. D., III. Brown and S. H. Koenig, *Magn. Reson. Med.*, **1986**, *3*, 242–250.
26. E. Balogh, Z. He, W. Hsieh, S. Liu and E. Tóth, *Inorg. Chem.*, **2007**, *46*, 238–250.
27. A. Bianchi, L. Calabi, C. Giorgi, P. Losi, P. Mariani, D. Palano, P. Paoli, P. Rossi and B. Valtancoli, *J. Chem. Soc., Dalton Trans.*, **2001**, 917–922.
28. S. Wang and T. D. Westmoreland, *Inorg. Chem.*, **2009**, *48*, 719–728.
29. L. Tei, G. Gugliotta, M. Fekete, F. K. Kálmán and M. Botta, *Dalton Trans.*, **2011**, *40*, 2025–2032.

30. J. E. Newton and F. C. Jackels, *J. Coord. Chem.*, **1988**, *19*, 265–277.
31. S. C. Jackels, M. M. Durham, J. E. Newton and T. C. Henninger, *Inorg. Chem.*, **1992**, *31*, 234–239.
32. *Purification of Laboratory Chemicals*; D. D. Perrin, Pergamon Press, Oxford, **1988**.
33. (a) E. P. Papadopoulos, A. Jarrar and C. H. Issidorides, *J. Org. Chem.*, **1966**, 615–616; (b) M. Hirano, S. Yakabe, H. Chikamori, J. H. Clark and T. Morimoto, *J. Chem. Res.*, **1998**, 770–771.
34. A. Bencini, L. Fabbrizzi and A. Poggi, *Inorg. Chem.*, **1981**, *20*, 2544–2549.
35. H. Gali, K. R. Prabhu, S. R. Karra and K. V. Katti, *J. Org. Chem.*, **2000,** *65*, 676–680.
36. L. W. Bieber and M. C. F. de Araújo, *Molecules*, **2002**, *7*, 902–906.
37. S. Aime, M. Botta, L. Frullano, S. Geninatti Crich, G. Giovenzana, R. Pagliarin, G. Palmisano, F. R. Sirtori and M. Sisti, *J. Med. Chem.*, **2000**, *43*, 4017–4024.
38. J. M. Siaugue, F. Segat-Dioury, I. Sylvestre, A. Favre-ReÂguillon, J. Foos, C. Madic and A. Guy, *Tetrahedron*, **2001**, *57*, 4713–4718.
39. W. Baker, K. M. Buggle, J. F. W. McOmie and D. A. M. Watkins, *J. Chem. Soc.*, **1958**, 3594–3603.
40. F. Dioury, C. Ferroud, A. Guya and M. Port, *Tetrahedron*, **2009**, *65*, 7573–7579.
41. G. R. Newkome, S. Pappalardo, V. K. Gupta and F. R. Fronczek, *J. Org. Chem.*, **1983**, *48*, 4848–4851.
42. M. Ouchi, Y. Inoue, T. Kanzaki and T. Hakushi, *J. Org. Chem.*, **1984**, *49*, 1408–1412.
43. J. E. Richman and T. J. Atkins, *J. Am. Chem. Soc.*, **1974**, *26*, 2268–2270.
44. V. J. Thöm, M. S. Shaikjee and R. D. Hancock, *Inorg. Chem.*, **1986**, *25*, 2992–3000.
45. O. Storm and U. Lüning, *Chem. Eur. J.*, **2002**, *8*, 793–798.
46. F. Bonadio, M.-C. Senna, J. Ensling, A. Sieber, A. Neels, H. Stoeckli-Evans and S. Decurtins, *Inorg. Chem.*, **2005**, *44*, 969–978.
47. J. Notni, P. Hermann, J. Havlíčková, J. Kotek, V. Kubíček, J. Plutnar, N. Loktionova, P. J. Riss, F. Rösch and I. Lukeš, *Chem. Eur. J.*, **2010**, *16*, 7174–7185.
48. V. Kubíček, J. Havlíčková, J. Kotek, G. Tircsó, P. Hermann, E. Tóth and I. Lukeš, *Inorg. Chem.*, **2010**, *49*, 10960–10969.
49. M. Kývala and I. Lukeš, *International Conference Chemometrics '95*, Pardubice, Czech Republic, **1995**, p. 63
50. M. Kývala, P. Lubal and I. Lukeš, *IX. Spanish–Italian and Mediterranean Congress on Thermodynamics of Metal Complexes (SIMEC 98)*, Girona, Spain, 1998. The full version of the OPIUM program is available (free of charge) on http://web.natur.cuni.cz/~kyvala/opium.html
51. (a) A. E. Martell and R. M. Smith, *Critical Stability Constants*, Vols. 1–6. Plenum Press, New York, **1974**–**1989**; (b) NIST Standard Reference Database 46 (Critically Selected Stability Constants of Metal Complexes), Version 7.0, **2003**; (c) C. F. Baes, Jr., and R. E. Mesmer, *The Hydrolysis of Cations*, Wiley, New York, **1976**.
52. (a) M. Försterová, I. Svobodová, P. Lubal, P. Táborský, J. Kotek, P. Hermann and I. Lukeš, *Dalton Trans.*, **2007**, 535–549; (b) V. Kubíček, J. Kotek, P. Hermann and I. Lukeš, *Eur. J. Inorg. Chem.*, **2007**, 333–344.
53. D. S. Raiford, C. L. Fisk and E. D. Becker, *Anal. Chem.*, **1979**, *51*, 2050–2051.
54. R. L. Vold, J. S. Waugh, M. P. Klein and D. E. Phelps, *J. Chem. Phys.*, **1968**, *48*, 3831–3832.
55. S. Meiboom and D. Gill, *Rev. Sci. Instrum.*, **1958**, *29*, 688–691.
56. A. D. Hugi, L. Helm and A. E. Merbach, *Helv. Chim. Acta*, **1985**, *68*, 508–521.
57. Z. Otwinowski and W. Minor, *HKL Denzo and Scalepack Program Package by Nonius BV*, Delft, **1997**; Z. Otwinowski and W. Minor, *Methods Enzymol.*, **1997**, *276*, 307–326.

58. *SIR92. Program for Automatic Solution of Crystal Structures by Direct Methods*; A. Altomare, G. Cascarano, C. Giacovazzo, A. Guagliardi, M. C. Burla, G. Polidori and M. Camalli, *J. Appl. Cryst.*, **1994**, *27*, 435–435.
59. G. M. Sheldrick, *SHELXL97. Program for Crystal Structure Refinement from Diffraction Data*, University of Göttingen, Göttingen **1997**.
60. *Scientist for Windows* version 2.0, Micromath Inc., Salt Like City, UT, **1995**.
61. M. F. Cabral, J. Costa, R. Delgado, J. J. R. Frausto de Silva and M. F. Vilhena, *Polyhedron*, **1990**, *9*, 2847–2857.
62. W. Clegg, P. B. Iveson and J. C. Lockhart, *Dalton Trans.*, **1992**, 3291–3298.
63. I. Lukeš, J. Kotek, P. Vojtíšek and P. Hermann, *Coord. Chem. Rev.*, **2001**, *216–217*, 287–312.
64. D. P. Riley, S. L. Henke, P. J. Lennon, R. H. Weiss, W. L. Neumann, W. J., Jr. Rivers, K. W. Aston, K. R. Sample, H. Rahman, C.-S. Ling, J.-J. Shieh, D. H. Busch and W. Szulbinski, *Inorg. Chem.*, **1996**, *35*, 5213–5231.
65. A. Dees, A. Zahl, R. Puchta, N. J. R. van Eikema Hommes, F. W. Heinemann and I. Ivanović-Burmazović, *Inorg. Chem.*, **2007**, *46*, 2459–2470.
66. M. F. Cabral and R. Delgado, *Helv. Chim. Acta*, **1994**, *77*, 515–524.
67. J. Costa and R. Delgado, *Inorg. Chem.*, **1993**, *32*, 5257–5265.
68. R. Yang and L. J. Zompa, *Inorg. Chem.*, **1976**, *15*, 1499–1502.
69. I. Lázár, R. Király and Z. Takács, *J. Coord. Chem.*, **2000**, *51*, 293–304.
70. C. F. G. C. Geraldes, A. D. Sherry and W. P. Cacheris, *Inorg. Chem.*, **1989**, 28 (17), 3336–3341.
71. A. S. Fernandes, M. F. Cabral, J. Costa, M. Castro, R. Delgado, M. G. B. Drew and V. Félix, *J. Inorg. Biochem.*, **2011**, *105*, 410–419.
72. E. Brücher and A. D. Sherry, *Inorg. Chem.*, **1990**, *29*, 1555–1559.
73. E. Tóth, E. Brücher, I. Lázár and I. Tóth, *Inorg. Chem.*, **1994**, *33*, 4070–4076.
74. L. Sarka, L. Burai and E. Brücher, *Chem. Eur. J.*, **2000**, *6*, 719–724.
75. E. Balogh, R. Tripier, R. Ruloff and E. Tóth, *Dalton Trans.*, **2005**, 1058–1065.
76. G.-F. Liu, M. Filipović, F. W. Heinemann and I. Ivanović-Burmazović, *Inorg. Chem.*, **2007**, *46*, 8825–8835.
77. Y. Fukuda, M. Hirota, M. Kon-no, A. Nakao and K. Umezawa, *Inorg. Chim. Acta*, **2002**, *339*, 322–326.
78. Y. Ducommun, K. E. Newmann and A. E. Merbach, *Inorg. Chem.*, **1980**, *19*, 3696–3703.
79. I. Bertini, F. Briganti, Z. Xia and C. J. Luchinat, J. Magn. Reson., Ser. A, **1993**, *101*, 198–201.
80. M. S. Zetter, M. Grant, E. J. Wood, H. W. Dodgen and J. P. Hunt, *Inorg. Chem.*, **1972**, *11*, 2701–2706.
81. J. Maigut, R. Meier, A. Zahl and R. van Eldik, *J. Am. Chem. Soc.*, **2008**, *130*, 14556–14569.
82. (a) S. Aime, M. Botta, J. I. Bruce, V. Mainero, D. Parker and E. Terreno, *Chem. Commun.*, **2001**, 115–116; (b) J. I. Bruce, R. S. Dickins, L. J. Govenlock, T. Gunnlaugsson, S. Lopinski, M. P. Lowe, D. Parker, R. D. Peacock, J. J. B. Perry, S. Aime and M. Botta, *J. Am. Chem. Soc.*, **2000**, *122*, 9674–9684.

Appendixes

Appendix 1 **p. 67–96**

B. Drahoš, J. Kotek, P. Hermann, I. Lukeš and E. Tóth „*Mn^{2+} Complexes with Pyridine-Containing 15-Membered Macrocycles: Thermodynamic, Kinetic, Crystallographic, and $^{1}H/^{17}O$ Relaxation Studies*“
Inorg. Chem., **2010**, *49*, 3224–3238.

Appendix 2 **p. 97–108**

B. Drahoš, V. Kubíček, C. S. Bonnet, P. Hermann, I. Lukeš and E. Tóth „*Dissociation kinetics of Mn^{2+} complexes of NOTA and DOTA*“
Dalton Trans., **2011**, *40*, 1945–1951.

Appendix 3 **p. 109–129**

B. Drahoš, M. Pniok, J. Kotek, P. Hermann, I. Lukeš and E. Tóth „*Mn^{2+} complexes of 1-oxa-4,7-diazacyclononane based ligands with acetic, phosphonic and phosphinic acid pendant arms: stability and relaxation studies*”
Dalton Trans., **2011** – accepted.

Appendix 4 **p. 131–175**

B. Drahoš, J. Kotek, I. Císařová, P. Hermann, L. Helm, I. Lukeš and E. Tóth “*Mn^{2+} complexes with 12-membered pyridine based macrocycles bearing carboxylate or phosphonate functions – crystallographic, thermodynamic, kinetic, redox and $^{1}H/^{17}O$ relaxation studies*”
– in preparation